El Niño Modoki and its possible teleconnection

Karumuri Ashok,[1,2] Swadhin K. Behera,[1] Suryachandra A. Rao,[1] Hengyi Weng,[1] and Toshio Yamagata[1,3]

Received 4 July 2006; revised 2 March 2007; accepted 13 June 2007; published 8 November 2007.

[1] Using observed data sets mainly for the period 1979–2005, we find that anomalous warming events different from conventional El Niño events occur in the central equatorial Pacific. This unique warming in the central equatorial Pacific associated with a horseshoe pattern is flanked by a colder sea surface temperature anomaly (SSTA) on both sides along the equator. empirical orthogonal function (EOF) analysis of monthly tropical Pacific SSTA shows that these events are represented by the second mode that explains 12% of the variance. Since a majority of such events are not part of El Niño evolution, the phenomenon is named as El Niño Modoki (pseudo-El Niño) (''Modoki'' is a classical Japanese word, which means ''a similar but different thing''). The El Niño Modoki involves ocean-atmosphere coupled processes which include a unique tripolar sea level pressure pattern during the evolution, analogous to the Southern Oscillation in the case of El Niño. Hence the total entity is named as El Niño–Southern Oscillation (ENSO) Modoki. The ENSO Modoki events significantly influence the temperature and precipitation over many parts of the globe. Depending on the season, the impacts over regions such as the Far East including Japan, New Zealand, western coast of United States, etc., are opposite to those of the conventional ENSO. The difference maps between the two periods of 1979–2004 and 1958–1978 for various oceanic/atmospheric variables suggest that the recent weakening of equatorial easterlies related to weakened zonal sea surface temperature gradient led to more flattening of the thermocline. This appears to be a cause of more frequent and persistent occurrence of the ENSO Modoki event during recent decades.

Citation: Ashok, K., S. K. Behera, S. A. Rao, H. Weng, and T. Yamagata (2007), El Niño Modoki and its possible teleconnection, *J. Geophys. Res.*, *112*, C11007, doi:10.1029/2006JC003798.

1. Introduction

[2] From the point of climate variability, the year 2004 was very unusual. We start from mentioning some examples. During the summer of that year from June to September, southern India, along with some parts of northern India experienced droughts (Figure 1a). Parts of Japan as well as Korea also experienced severe drought and heat wave, while Philippine Islands received surplus rainfall. A large part of Australia experienced deficit in austral winter rainfall. Tasmania and New Zealand, on the other hand, received surplus precipitation. Southern Mexico and Ecuador regions suffered from drought, whereas northern Brazil received surplus rainfall. We notice that sea surface temperature anomalies (SSTA) in the equatorial Pacific showed a peculiar zonal tripole pattern (Figure 1b): While the central tropical Pacific was warmer than normal, it was flanked by anomalously cooler SSTA to its east and west. This anomalous SSTA pattern is different from that during typical El Niño events [e.g., *Rasmusson and Carpenter*, 1982]. The condition continued through the following boreal winter (figure not shown).

[3] In 2003, the National Oceanic and Atmospheric Administration (NOAA) of the United States of America revised the definition of El Niño ''as a phenomenon in the equatorial Pacific Ocean characterized by a positive sea surface temperature departure from normal (for the 1971–2000 base period) in the Niño 3.4 region (see Table 1 for definition) greater than or equal in magnitude to 0.5°C, averaged over three consecutive months.'' (Details can be found at http://www.noaanews.noaa.gov/stories/s2095.htm. The definition has been adopted by the World Meteorological region IV [*Larkin and Harrison*, 2005a].) *Larkin and Harrison* [2005a] refer to this redefined El Niño as ''Dateline El Niño'' and mention that the warming may not reach NINO3 region during Dateline El Niño events. Interestingly, the 2004 event is not exactly covered by this definition because the warmer central region extends from the western fringe of the NINO4 region rather than being just confined to the NINO3.4 region (Figure 1b). Moreover, the western Pacific and eastern Pacific SST anomalies during the boreal summer of 2004 were significantly colder than normal

[1] Frontier Research Center for Global Change/JAMSTEC, Yokohama, Kanagawa, Japan.
[2] Now at APEC Climate Center, Busan, Republic of Korea.
[3] Department of Earth and Planetary Science, Graduate School of Science, University of Tokyo, Tokyo, Japan.

0148-0227/07/2006JC003798

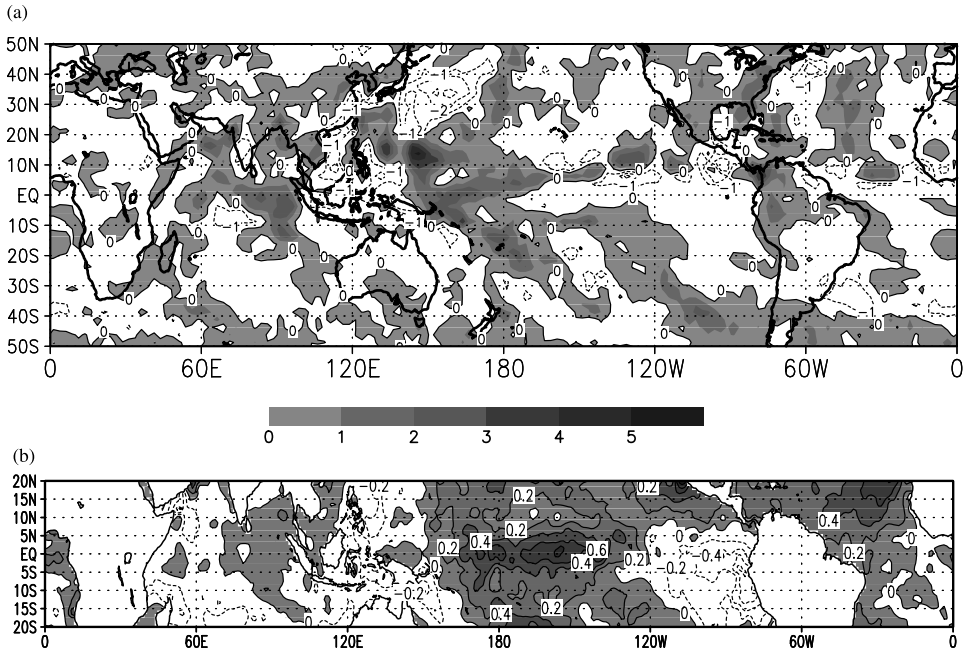

Figure 1. Anomalous conditions during JJAS 2004 (a) for rainfall in cm/month and (b) SST in °C. The data sets of Version 2 Global Precipitation Climatology Project Monthly Precipitation Analysis [*Adler et al.*, 2003], and the Hadley Centre Global Sea Ice and Sea Surface Temperature (HadISST) Analyses [*Rayner et al.*, 2003] for the period 1979–2004 were used to obtain Figures 1a and 1b, respectively.

(K. Ashok et al., An unusual coupled mode in the tropical Pacific during 2004, manuscript in preparation, 2007; available at http://www.jamstec.go.jp/frsgc/research/d1/iod/). In particular, the magnitude of the cooler than normal SSTA in the eastern tropical Pacific is comparable to that of the warmer central pole. Given the maximum boreal summer warming in central tropical Pacific distinctly persisted through the following boreal winter (K. Ashok et al., manuscript in preparation, 2007), it is not surprising that experts have started debating on whether to classify that year as an El Niño year (World Meteorological Organization, El Niño update, 20 April 2005). The peculiarity of events such as the 2004 event was also noticed by *Donguy and Dessier* [1983] and *Meyers et al.* [2007]. In fact, hints for existence of the interesting SSTA pattern in the tropical Pacific that is different from ENSO are also found in earlier works such as those by *Weare et al.* [1976] and *Meyers et al.* [1999].

[4] Because of the obvious distinction from the traditional El Niño [*Rasmusson and Carpenter*, 1982] and even from that defined by NOAA in 2003, we refer to the SSTA pattern observed in 2004, namely, warming in the central Pacific (∼NINO4 region) flanked by colder SSTA to the west and east, as an El Niño Modoki (pseudo-El

Table 1. Definitions of Different Regions/SSTA-Based Indices Used in This Study

Index Name	Definition
NINO3.4	the region is bounded by (5°N–5°S, 170°W–120°W); the area-averaged sea surface temperature anomaly (SSTA) over this region is known as NINO3.4 index
NINO3	the region is bounded by (5°N–5°S, 150°W–90°W); the area-averaged sea surface temperature anomaly over this region is known as NINO3 index, which is a well-known ENSO index
NINO1+2	the region is bounded by (equator to 10°S, 90°W–80°W); the area-averaged sea surface temperature anomaly over this region is known as NINO1+2 index
NINO4	the region is bounded by (5°N–5°S, 160°E–150°W); the area-averaged sea surface temperature anomaly over this region is known as NINO4 index
Trans-Nino index	defined as difference between normalized SSTA between NINO4 and NINO1+2 [*Trenberth and Stepaniak*, 2001]
Indian Ocean Dipole Mode Index	the Indian Ocean Dipole Mode Index (IODMI) is defined as the SSTA difference between the western (50°E–70°E, 10°S–10°N) and southeastern (90°E–110°E, 10°S to equator) regions of the tropical Indian Ocean [*Saji et al.*, 1999]
Subtropical Dipole Mode Index	the Indian Ocean Subtropical Dipole Mode Index (SDI) is defined as the SSTA difference between the western subtropical (55°E–65°E, 37°S–27°S) and southeastern (90°E–100°E, 28°S–18°S) regions of the subtropical Indian Ocean [*Behera and Yamagata*, 2001]
El Niño Modoki index	see the details in the text that follows equation (1) of this paper

Niño) event; this term is now popular in Japan and east Asia. (The word Modoki was introduced by T. Yamagata during 2004 while explaining a probable cause behind the abnormal summer climatic conditions over Japan. It has been often used since then by various Japanese Mass Media. ''Modoki'' is a classical Japanese word which means ''similar but different.'' A news article also appeared in *The Japan Times* on 24 July 2004 under the heading '''Mock El Nino' culprit behind heat wave, floods: Professor,'' which follows: ''The heat wave and floods in various parts of Japan are being caused by an El Nino-like phenomenon in the central Pacific Ocean, a Japanese researcher said Friday. Toshio Yamagata, a professor at the University of Tokyo specializing in climate dynamics, said an increase in the sea surface temperature has activated convection currents and promoted a high-pressure ridge in the Pacific, bringing a hot summer to Japan . . .'' For further details of this news, see http://www.japantimes.co.jp/cgi-bin/getarticle.pl5?nn20040724f3.htm.) We believe that identifying a unique phenomenon with the most appropriate definition, just as new species in biology, is important to promote further research. This is a key issue of the present study.

[5] This paper is composed of four sections. The data sets and methods of analysis are briefly described in section 2. Section 3 discusses the analyzed results, where we justify the reason for classifying the phenomenon in 2004 and other similar ones as an entity different from the conventional El Niño and even the so-called dateline El Niño. The possible teleconnections of the typical SSTA pattern associated with the El Niño Modoki (pseudo-El Niño) are identified, along with a discussion on the mechanism for formation of the unique SSTA pattern and that for teleconnections. This further verifies the novel aspect of the present research. Section 4 is reserved for discussion on why such an event as in 2004 occurs more frequently since the late 1970s and suggests a possible link with the recent global warming. The summary and concluding remarks are presented in section 5.

2. Data Sets and Methods of Analysis

[6] The Hadley Centre Global Sea Ice and Sea Surface Temperature (HadISST) analyses data sets [*Rayner et al.*, 2003] from January 1958 to February 2005 are used in this study. For verification, we also use the Optimally Interpolated Sea Surface Temperature (OISST) data sets [*Reynolds et al.*, 2002] for the period from January 1982 through March 2005. For precipitation analysis, we mainly use the Version 2 Global Precipitation Climatology Project (GPCP) Monthly Precipitation Analysis [see *Adler et al.*, 2003, and references therein] for the period from 1979 through 2004. The results are verified by the use of Climate Prediction Center Merged Analysis of Precipitation (CMAP) data [*Xie and Arkin*, 1996] for the same period; unless specifically mentioned, all the discussion in this study related to precipitation analysis is based on GPCP data sets. The National Centers for Environmental Prediction/National Center for Atmospheric Research (NCEP/NCAR) reanalysis products [*Kalnay et al.*, 1996] such as the sea level pressure, geopotential, and wind data sets from 1958 through 2005 are also employed in this study. We also use the surface wind data sets from European Centre for Medium-range Weather Forecasts reanalysis (ERA 40 [*Simmons and Gibson*, 2000]) available from January 1958 till August 2002 for verification of decadal trends in low-level equatorial zonal winds over the tropical Pacific. The recent ocean heat content data sets for the upper ocean down to 300 m depth [*Levitus et al.*, 2005] are used to assess the long-term changes. We also utilize the sea surface height (SSH) data derived from Simple Ocean Data Assimilation (SODA) product for the period from 1979 through 2004 [*Carton et al.*, 2005; *Carton and Giese*, 2007].

[7] The present analysis covers basically the ocean and atmospheric data from January 1979 to February 2005 (December 2004 for GPCP and CMAP data sets), unless specified otherwise. Anomalies are deviations from climatology in the above base period. The reason for choosing the post-1978 data is twofold. The first is availability of better and more reliable data quality, particularly in National Centers for Environmental Prediction/National Center for Atmospheric Research global reanalysis data (NCEP/NCAR [*Kalnay et al.*, 1996]) data set over the Southern Hemisphere (see *Kistler et al.* [2001] and *Trenberth et al.* [2001] for details); also, some of the data sets such as the CMAP data [*Xie and Arkin*, 1996] are only available from 1979. The second is that by using data sets from 1979, we avoid necessity of stratifying events before and after the Pacific regime shift (see *Nitta and Yamada* [1989], *Stephens et al.* [2001], *Deser et al.* [2004], and *Hartmann and Wendler* [2005] for details and further references) that occurred around the middle of 1970s.

[8] Further, we use the NCEP/NCAR 2 m temperature data sets to examine the potential impacts of the El Niño Modoki. As the reanalysis for this parameter is to some extent dependent on model parameterizations used in the reanalysis, we have also analyzed the observed Climate Research Unit (CRUTEM3) monthly land surface temperature [*Jones et al.*, 1999] available at $5^\circ \times 5^\circ$. For the period 1979–2004 to validate the NCEP/NCAR 2 m temperature data sets.

[9] We first carry out an empirical orthogonal function (EOF) analysis, using singular value decomposition (SVD), on SSTA to identify modes of variability relevant to the El Niño Modoki (pseudo-El Niño) pattern as observed in summer of 2004; the dominant two patterns obtained from the EOF analysis are confirmed by a complex EOF analysis (see Appendix A). We then try to extract the apparent teleconnection patterns using partial correlation technique (see Appendix B for details) and composite analysis. Each of the monthly indices and anomaly fields have been seasonally averaged over a period from June to September, and December to February to obtain what we hereafter refer to as the boreal summer and winter values, respectively. The significance levels for composite and partial correlation analyses were obtained by the standard two-tailed Student's *t* test; we have further verified the significant correlation zones by employing a Monte Carlo method with 1000 simulations (see Appendix B).

3. Variability Related to El Niño Modoki

3.1. Climate Modes of the Tropical Pacific Variability

[10] The first four leading EOF modes of the monthly SSTA over the tropical Pacific region are presented in Figure 2. The EOF1 pattern shown in Figure 2a captures

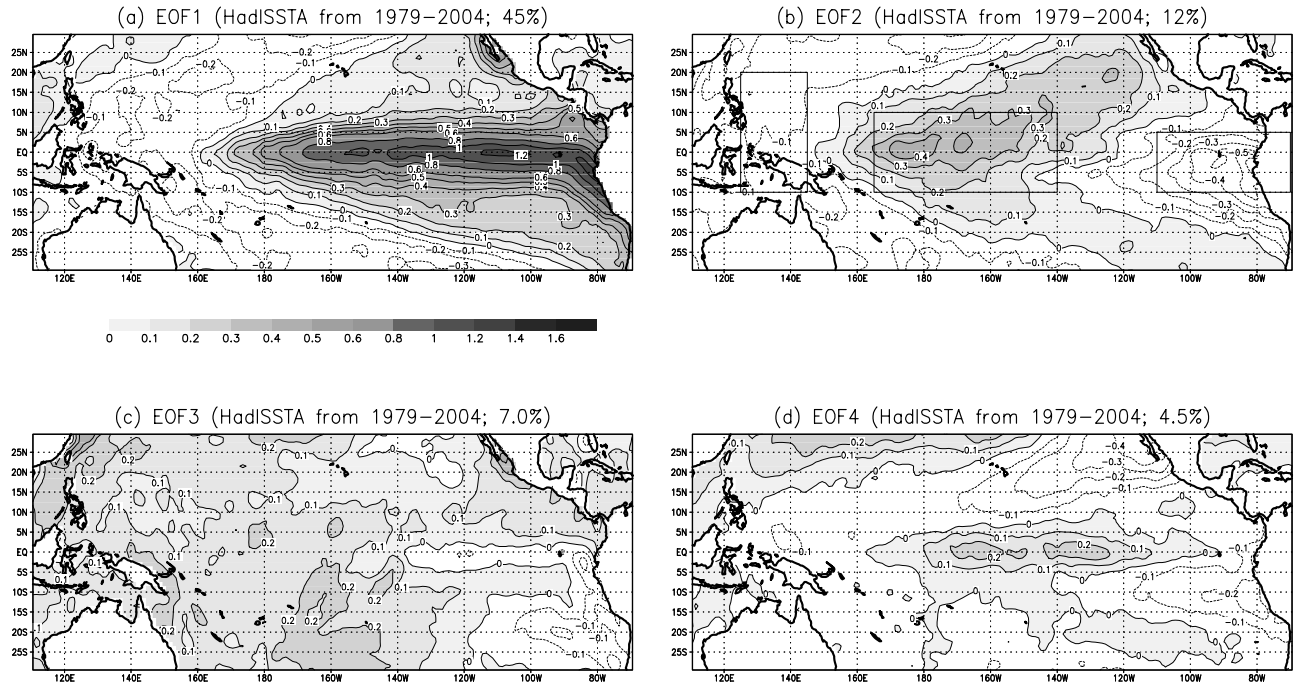

Figure 2. Top four EOF modes of tropical Pacific SSTA (1979–2004) multiplied by respective standard deviations of the principal components; units in °C.

the well-known El Niño pattern [*Rasmusson and Carpenter*, 1982]. This mode explains about 45% of the tropical Pacific SST variability for the period between 1979 and 2004. The EOF2 that explains 12% of the SST variability captures a zonal tripole pattern in the tropical region (Figure 2b). Both eastern and western tropical Pacific SSTAs have loadings of the same sign, while those of the central tropical Pacific are opposite. In higher latitudes, the positive loadings in the central equatorial Pacific spread eastward in both hemispheres, and this horseshoe pattern straddles the tongue of negative loadings in the equatorial eastern Pacific. The magnitudes of the loadings in the central and eastern Pacific are comparable. The SSTA for the summer of 2004 shown in Figure1b is similar to this EOF2 pattern. In particular, the SSTA pattern continued till the end of boreal winter in 2004. There are several other years such as 1980, 1986, 1990, 1991, 1994, 2002 when an anomaly pattern similar to that in Figure 2b (and Figure 1b) is observed. As the variances explained by the first two EOF patterns are well separated [*North et al.*, 1982] and are supported by the results from the complex EOF analysis discussed later in this section as well as in the Appendix A, it is reasonable to expect that these two patterns represent different modes of climate variability. Therefore we refer to the EOF2 SSTA pattern associated with the positive phase of its principal component (Figure 3) as an El Niño Modoki (pseudo-El Niño) event. Consequently, in analogy with the nomenclature of El Niño events, we refer to a reversed event such as in 1998 with the anomalously cold SSTA in the central equatorial and subtropical Pacific flanked by the warmer than normal SSTA on both sides along the equator (figure not shown) as an La Niña Modoki (pseudo-La Niña) event.

[11] The EOF3 and EOF4 patterns (Figures 2c and 2d) explain only about 7% and 4.6% of the variance, respectively. (The results from a similar EOF analysis of the linearly detrended tropical SST data sets (figures not shown) do not change the properties of the top two modes much, except that the variance explained by the EOF1 rises to 47%. However, the present EOF3 disappears completely, indicating that the EOF3 is nothing but the background trend.) We repeated the EOF analysis with the OISST [*Reynolds et al.*, 2002] data sets from 1982 through 2005, and the results are well in agreement with the aforementioned findings. The robustness of the EOF patterns was also examined by confining the meridional domain to 10°S–10°N (figures not shown); the EOF2 pattern in the tropics and the associated tropical Pacific SSTA variance do not change significantly even for the meridional domain expanded to 45°S–45°N (figure not shown). The tripolar structure of the second mode of tropical Pacific SSTA

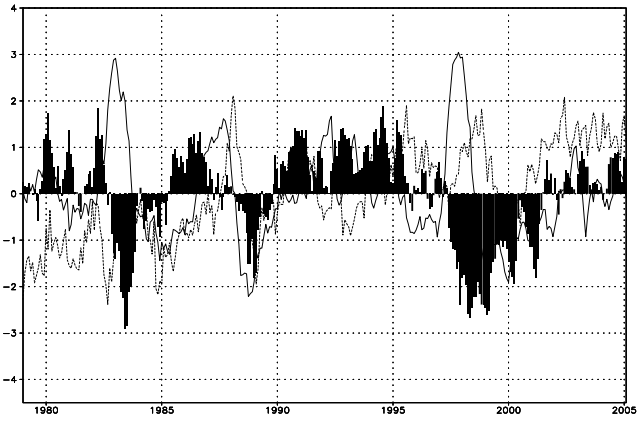

Figure 3. Normalized time series of PC1 (solid line), PC2 (bar), and PC3 (dashed line).

variability was also verified by Varimax rotation [after *Richman*, 1986] of first 10 EOF modes (figures not shown). Further, from the tropical SSTA, we removed the reconstructed EOF1 component that was obtained by multiplying the EOF1 loadings (Figure 2a) with the associated PC1. An EOF analysis of the remainder indicates that the EOF1 and its principal component obtained from this exercise strongly resemble (figures not shown) those of the EOF2 of the total SSTA shown in Figure 2a. The variance explained by this El Niño Modoki-associated mode increases to 21% in the absence of ENSO-related EOF1 signal. This exercise further demonstrates the robustness of the EOF2 mode and indicates that El Niño Modoki may be independent of the ENSO signal.

[12] We also carried out a complex EOF (CEOF) analysis on the tropical Pacific SSTA and SODA sea surface height anomalies (SSHA) to get the propagation characteristics of these events. The real component of the complex EOF1 and EOF2 are similar to those shown in Figures 2a and 2b (figures not shown). The phase diagram of the CEOF1 (Figure A1 shown in Appendix A) demonstrates that the phase of the CEOF1 propagates mainly from west to east prominently in the equatorial regions confirming the importance of oceanic Kelvin waves for El Niño. Unlike the phase of first CEOF mode of SSH, phase for the second mode propagates from east to west in the off-equatorial regions and west to east in the central equatorial Pacific, suggesting that the off-equatorial Rossby waves and equatorial Kelvin waves are involved in the formation of El Niño Modoki event; this distinct aspect is discussed further in section 3.2. The amplitudes of the complex EOF are provided in Figures A2.

[13] The time series of the normalized principal components (PCs) of EOF1, EOF2, and EOF3 are presented in Figure 3. The correlation between PC1 and PC2 is zero by definition. A cross-correlation analysis between PC1 and PC2 at different leads and lags gives a maximum correlation of 0.43 with PC2 leading PC1, indicating that substantial percentages of the variances explained by the EOF2 and EOF1 are not explained by each other during the study period.

[14] The correlation between PC1 and NINO3 index is very high, and amounts to 0.98, which proves that EOF1 represents the conventional El Niño well. On the other hand, the correlation between PC2 and NINO3 index is very low (−0.09). All these prove that the El Niño Modoki events are not related to the conventional El Niño events. The El Niño Modoki needs to be addressed as a unique phenomenon in the tropical Pacific. The correlation between the NINO4 index and PC2 is 0.51. This significant correlation is expected to some extent because the central pole of the EOF2 is located around the NINO4 region. The correlation between the NINO3 and NINO4 indices is 0.73. Since the NINO4 SST index is related to both indices of the El Niño and El Niño Modoki, we need to be careful when we use the NINO4 index as a conventional ENSO index, at least after 1978. The correlation between NINO1+2 index and PC2 is 0.44. The correlation between NINO3.4 index and the PC2 is 0.19, which is rather small; this demonstrates that the El Niño Modoki events are different even from the so-called "Dateline ENSO" events. The correlation of the PC2 with the Indian Ocean Dipole Mode Index [*Saji et al.*, 1999] and the Subtropical Dipole Mode Index [*Behera and Yamagata*, 2001] are only 0.1 and 0.15, respectively.

[15] On the basis of the EOF2 pattern presented in Figure 2b and the PC2 time series shown in Figure 3, we derive an El Niño Modoki index (EMI). Because of the unique tripolar nature of the SSTA, the index is defined as follows:

$$\mathrm{EMI} = [\mathrm{SSTA}]_A - 0.5^{*}[\mathrm{SSTA}]_B - 0.5^{*}[\mathrm{SSTA}]_C \qquad (1)$$

The brackets in equation (1) represent the area-averaged SSTA over each of the region A (165°E–140°W, 10°S–10°N), B (110°W–70°W, 15°S–5°N), and C (125°E–145°E, 10°S–20°N), respectively. The time series of the EMI is shown in Figure 4a. The correlation between this new time series and the PC2 is 0.91, which is statistically significant at a 99% confidence level from a two-tailed Student's *t* test. This strong correlation shows that the index introduced here is appropriate to represent the El Niño Modoki events of the tropical Pacific. To examine its relationship with other indices in the tropical and subtropical Indo-Pacific regions, various correlation values are shown in Table 2.

[16] *Trenberth and Stepaniak* [2001] introduced another index called Trans-Nino index (TNI) as the difference between normalized SSTA between NINO4 and NINO1+2. TNI is correlated at 0.8 with the time series of SVD2 of SSTA and several atmospheric fields such as precipitation [*Trenberth et al.*, 2002a], and hence they accept TNI as an index (see Figure 4b) to represent the SVD2 in tropical Pacific; the correlation of the SVD2 time series with tropical Pacific SSTA resembles that of our EOF2 shown in Figure 2. The correlation between TNI and EMI is −0.87 for the study period. From this simple analysis, TNI appears to be almost the same with EMI. Nevertheless, we will show the advantage of EMI in the following. The correlations of the PC2 with NINO4 and NINO1 +2 indices are 0.51 and −0.44, respectively. On the other hand, its correlations with SSTA in our equivalent boxes A and B (see equation (1)) in the central and eastern tropical Pacific are 0.51 and −0.42. Up to that, both indices are similar. However, the correlation of the PC2 with our western box (box C defined in equation (1)) is −0.453, stronger in amplitude than that with NINO1+2, the eastern box of SSTA defining the TNI. This demonstrates that the western tropical Pacific SSTA is just as important as that of the eastern Pacific; this important aspect must be taken in to account in introducing a new index capturing the EOF2 type of phenomena in the tropical Pacific. Although the variances of SSTA contributing to the EOF2 in the tropical western Pacific are weaker than those in the tropical eastern Pacific, they are important because events such as 2004 are triggered in the western tropical Pacific (see K. Ashok et al., manuscript in preparation, 2007); this aspect is important for predicting the El Niño Modoki, and will be discussed in detail in section 3.4.3. Because of this importance of the western tropical Pacific, it is also worth noticing that the correlation of the western tropical Pacific SSTA with EMI is −0.51, much higher in magnitude than the correlation of 0.25 with TNI. From all the above, the EMI seems to be, statistically as well as dynamically, a better index for capturing the EOF2 pattern of tropical Pacific SSTA variability. The relative correlations

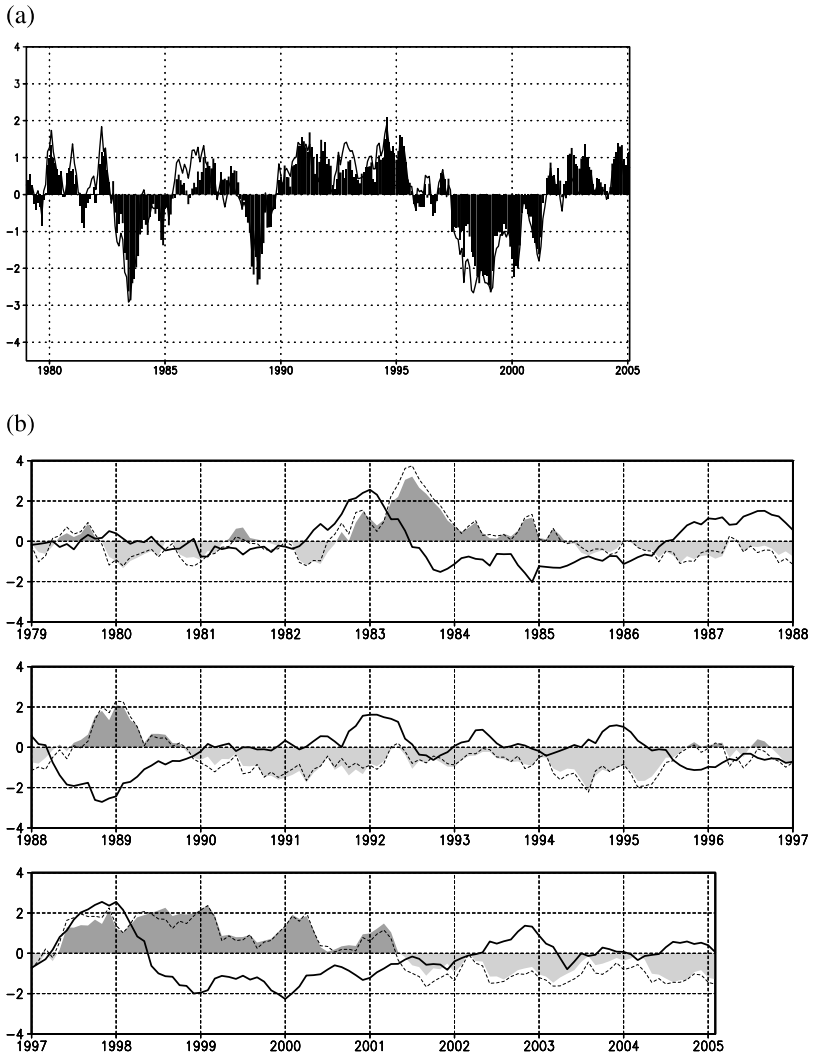

Figure 4. (a) Time series of normalized ENSO Modoki index (EMI; in bar) and that of the PC2 (thin line). The standard deviation of the EMI is 0.52°C. (b) Time series of Nino3.4 (solid thick line) index and TNI (dashed thin line) as defined by *Trenberth and Stepaniak* [2001]. Also shown is the time series of the inverted EMI (shaded). The sign of the EMI has been deliberately reversed to facilitate easy comparison of its evolution with the TNI.

of EMI and TNI with PC2 are 0.93 and 0.88, elucidating the slight superiority of EMI. However, because of their strong similarity and association with EOF2, both indices may be considered analogous in representation of the El Niño Modoki for many practical purposes, just as the NINO3 and NINO3.4 indices in case of El Niño events.

[17] *Trenberth and Stepaniak* [2001] and *Trenberth et al.* [2002a, 2002b] suggest that SSTA of the TNI type is only one aspect of ENSO evolution. In section 3.2, we demonstrate that this is unfortunately not correct for a majority of the events during the study period. This is the major difference between the present study and the important preceding work by *Trenberth and Stepaniak* [2001] and makes the present research unique.

[18] The correlation between the principal component of the EOF3 and EMI for the study period is only 0.24, indicating that EOF3 is not related El Niño Modoki. However, its potential role is further examined in section 4.

3.2. A Composite Picture of El Niño Modoki

[19] On the basis of the time series of the EMI shown in Figure 4a, we have identified seven typical El Niño Modoki events that lasted from boreal summer through boreal winter, peaking in one of these seasons (seasonal standard deviations for boreal summer and winter are 0.5°C and 0.54°C, respectively). (We call an El Niño Modoki event

Table 2. Correlation Values of the El Niño Modoki Index With Other Indices in the Tropical and Subtropical Indo-Pacific Region[a]

	EMI
NINO3	0.13
NINO4	0.73
NINO3.4	0.43
IODMI	0.06
SDI	0.02

[a]EMI, El Niño Modoki Index.

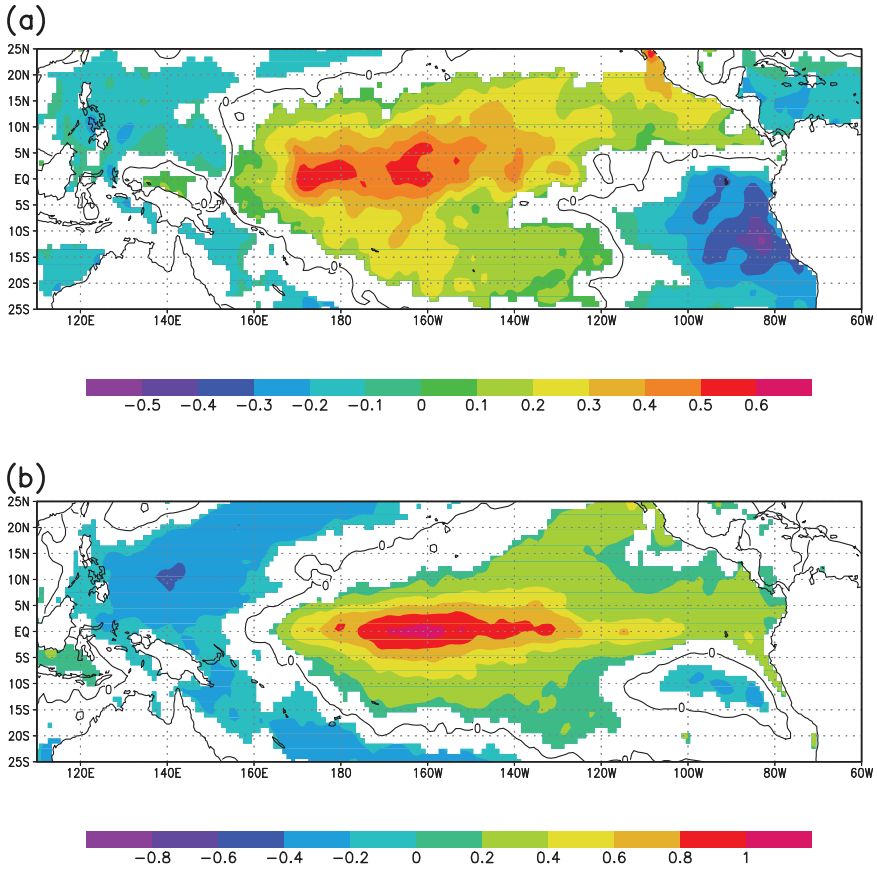

Figure 5. Composite SSTA in °C during strong positive El Niño Modoki events averaged over (a) seven boreal summers, namely, JJAS seasons of 1986,1990, 1991, 1992, 1994, 2002, and 2004, and (b) 8 boreal winters, namely, DJF seasons of 1979–1980, 1986–1987,1990–1991, 1991–1992, 1992–1993, 1994–1995, 2002–2003, and 2004–2005. Significant values above 95% confidence level from a two-tailed Student's *t* test are shaded.

"typical" when its amplitude of the index is equal to or greater than 0.7σ, where σ is the seasonal standard deviation.) These typical El Niño Modoki events occurred in 1986, 1990, 1991, 1992, 1994, 2002, and 2004. Additionally, we identified a typical El Niño Modoki during the boreal winter of 1979–1980 that lasted through the summer of 1980, though its amplitude fell below the threshold of 0.7σ by then. The SSTA patterns in these seven boreal summer seasons, and eight winter seasons including 1979–1980, have been composited for a common picture by removing high-frequency noise. The result is remarkable and shown in Figures 5a and 5b, respectively.

[20] During the boreal summer when an El Niño Modoki event occurs, the significantly warmer SSTA in the central equatorial Pacific is flanked by significantly colder-than-normal SSTA in the western and eastern tropical Pacific. This composite pattern for summer captures the EOF2 pattern presented earlier in Figure 2b quite well.

[21] The El Niño Modoki occurs not only in boreal summer months but also in boreal winter months from December to February (DJF). Figure 5b shows the composite SSTA in the boreal winter months. The composite pattern is qualitatively similar to that in summer (Figure 5a) and EOF2 (Figure 2b). The colder SSTA is relatively more widespread in the western tropical Pacific as compared to that in the eastern Pacific during boreal winter, whereas it is the other way round during boreal summer. The colder SSTA during boreal winter in the eastern tropical Pacific shifts southward due to spread of warmer anomalies from the central Pacific. We also note that El Niño Modoki events persisted from 1990 through 1994 with changing amplitude. The phenomenon was discussed previously as either protracted or prolonged El Niño in the literature [cf. *Allan et al.*, 2003].

[22] It is very interesting to note that during the El Niño Modoki events, the warmest SSTA does not propagate into the NINO1+2 region as they do during the conventional El Niño years such as 1987 and 1997 after the regime shift in the middle of 1970s (see discussion related to Figure 5 and *Tozuka and Yamagata* [2003] and K. Ashok et al. (manuscript in preparation, 2007)). Despite having identified the 2002 event in the tropical Pacific as a moderate El Niño event, *McPhaden* [2004, p. 690] also noted this aspect as in the following. "The pattern of SST anomalies was unusual, however, with the largest anomalies concentrated in the central equatorial Pacific in contrast to the relatively weak and short-lived warming in the eastern Pacific and along the west coasts of the Americas. Precisely what accounted for this SST anomaly pattern is unclear." *McPhaden* [2004] also noticed, in agreement with the present work, that the

spatial pattern of the SSTA resembled that during 1994–1995 but contrasted with 1997 El Niño; he also discussed the unique teleconnections during 2002.

[23] *Trenberth and Stepaniak* [2001] indicate that NINO3.4 and TNI are significantly correlated at different lags/leads, and hence they conclude that their SVD2 pattern is one phase of ENSO evolution. However, they admit that the relationship has changed along with changes in ENSO characteristics after the climate regime shift in the middle 1970s [*Nitta and Yamada*, 1989; *Stephens et al.*, 2001; *Deser et al.*, 2004; *Hartmann and Wendler*, 2005]. It is seen in the Figure 2 of *Trenberth and Stepaniak* [2001] that the lag/lead moving correlations have considerably weakened after 1976; these also changed their respective signs. Hence their conjecture that the El Niño Modoki pattern of SSTA is part of El Niño evolution [*Trenberth and Stepaniak*, 2001; *Trenberth et al.*, 2002a, 2002b] is not always supported. For example, K. Ashok et al. (manuscript in preparation, 2007) bring out distinctness of the 2004 El Niño Modoki event and point out that it cannot be described as part of the ENSO evolution. According to this study, it can be seen that, the time series of principal component of EOF2 as well as EMI are positive most of the time after March 2002 (also see Figure 4a). On the other hand, the time series of the NINO3 and NINO3.4 indices change their phase several times, and their amplitude is weak after 2002 (figures not shown; see K. Ashok et al., manuscript in preparation, 2007, Figure 4). Even during 2002, however, the EOF2 was dominant as compared to EOF1, as evidenced by the time series of the principal components (Figure 4a). Besides, the SSTA in the NINO4 region during this period was consistently warm (figure not shown; see K. Ashok et al., manuscript in preparation, 2007, Figure 2), indicating that the tropical Pacific was continuously in the positive phase of quasi-EOF2 mode condition since spring of 2002. If the hypothesis of *Trenberth and Stepaniak* [2001] applies, the El Niño Modoki conditions in summer of 2004 should have been followed (preceded) by an El Niño (a La Niña) after (before) 3–12 months; neither of these things happened, as indicated by the NINO3.4 index shown in Figure 4 or by the NINO3 index (see K. Ashok et al., manuscript in preparation, 2007, Figure 4). In fact, out of the three major El Niño events after 1977, only the 1982–1983 period fits the hypothesis stipulated by *Trenberth and Stepaniak* [2001]. Even during 1997 when a strong El Niño event occurred, it was preceded by a very weak El Niño Modoki event (see Figure 4b). Importantly, it can also be seen from Figure 4b that the condition suggested by *Trenberth and Stepaniak* [2001] is not valid for the so-called protracted El Niño period of 1990–1994.

[24] To further understand the relationship between El Niño Modoki and El Niño, a lead-lag analysis between the monthly values of the EMI and NINO3 index was carried out for the study period. It has turned out that EMI in April (October) is correlated at about 0.55 (0.45) with NINO3 index in December. On the other hand, February NINO3 index leads the August EMI with correlation of about 0.5. Similarly, Nino 3.4 index shows maximum correlation of 0.49 with EMI at 4 months lag. All these indicate that, after 1978, only up to a maximum of 30% of the total variance of either one of the El Niño Modoki and El Niño phenomena can be explained by the other. The analysis in this section clearly brings out the uniqueness of the El Niño Modoki events, and shows that they cannot be described as part of the El Niño evolution.

3.3. Coupled Processes of ENSO Modoki Events

[25] In this section, we discuss possible mechanisms for the evolution of the El Niño Modoki. To visualize the ocean-atmospheric coupled nature of the El Niño Modoki, we carry out lag/lead correlation analyses between EMI with various variables such as SSHA, wind stress anomalies, sea surface pressure anomalies, and ocean temperature anomalies at 10 m depth (T_{10}) from the SODA data sets [*Carton and Giese*, 2007, *Carton et al.*, 2005]; The near-surface temperature data of OISST [*Reynolds et al.*, 2002] were used in the SODA data set version 1.4.3 to update the mixed-layer temperature, and hence the impact from the heat flux boundary condition, provided by a bulk formula, is relatively unimportant [*Carton and Giese*, 2007]. Relatively high correlations between EMI and SSH anomalies are seen in the central and western tropical Pacific even at 12 months lag with the EMI lagging SSHA (Figure 6a). Positive (negative) correlation coefficients are observed in the central (western) Pacific. Coinciding with those, we also observe positive (negative) correlation coefficients for T_{10}. This appears to be excited by westerly wind anomalies in the western Pacific because those westerly wind anomalies, by transporting the warm water in the off-equatorial western Pacific to the equator, may drive downwelling equatorial Kelvin waves and induce deepening of the thermocline from the central to eastern Pacific. The wind anomalies are consistent with the surface pressure anomalies as seen in Figures 7a and 7b.

[26] In the following months, positive correlations with SSH anomalies become higher and propagate westward together with correlations of T_{10}. At 6 months lag, we observe easterly wind anomalies in the eastern Pacific in addition to the anomalous westerlies in the western Pacific (Figure 6c). Since these winds cause convergence in the central Pacific, the thermocline in central Pacific further deepens. With increasing easterlies in the eastern Pacific, the equatorial Rossby waves may deepen the thermocline off the equator and thus increase the warming in the central Pacific as indicated by the high correlations in the central Pacific at zero lag (Figure 6e). The evolution of the surface pressure anomalies is consistent again with the wind evolution (Figures 7c–7e). The vertical distribution of lag correlations between subsurface temperature anomalies averaged between 2°S and 2°N and EMI confirms the above picture (Figure 8). The warming in the central Pacific is thus strengthened owing to the arrival of downwelling equatorial Kelvin waves from the west and Rossby waves from the east. Highest correlations, in general, are found at subsurface depths at zero lag (Figure 8e) in equator and other near-equatorial latitudes (6°S–4°S, 2°N–4°N, 4°N–6°N, figures not shown), indicating that the SST warming in the central equatorial Pacific is due to those subsurface oceanic processes.

[27] After the peak of El Niño Modoki, anomalous easterlies in the eastern Pacific are further strengthened, and the equatorial upwelling is strengthened. The excited downwelling Rossby waves propagate further west and, together with the weakening westerlies in the western

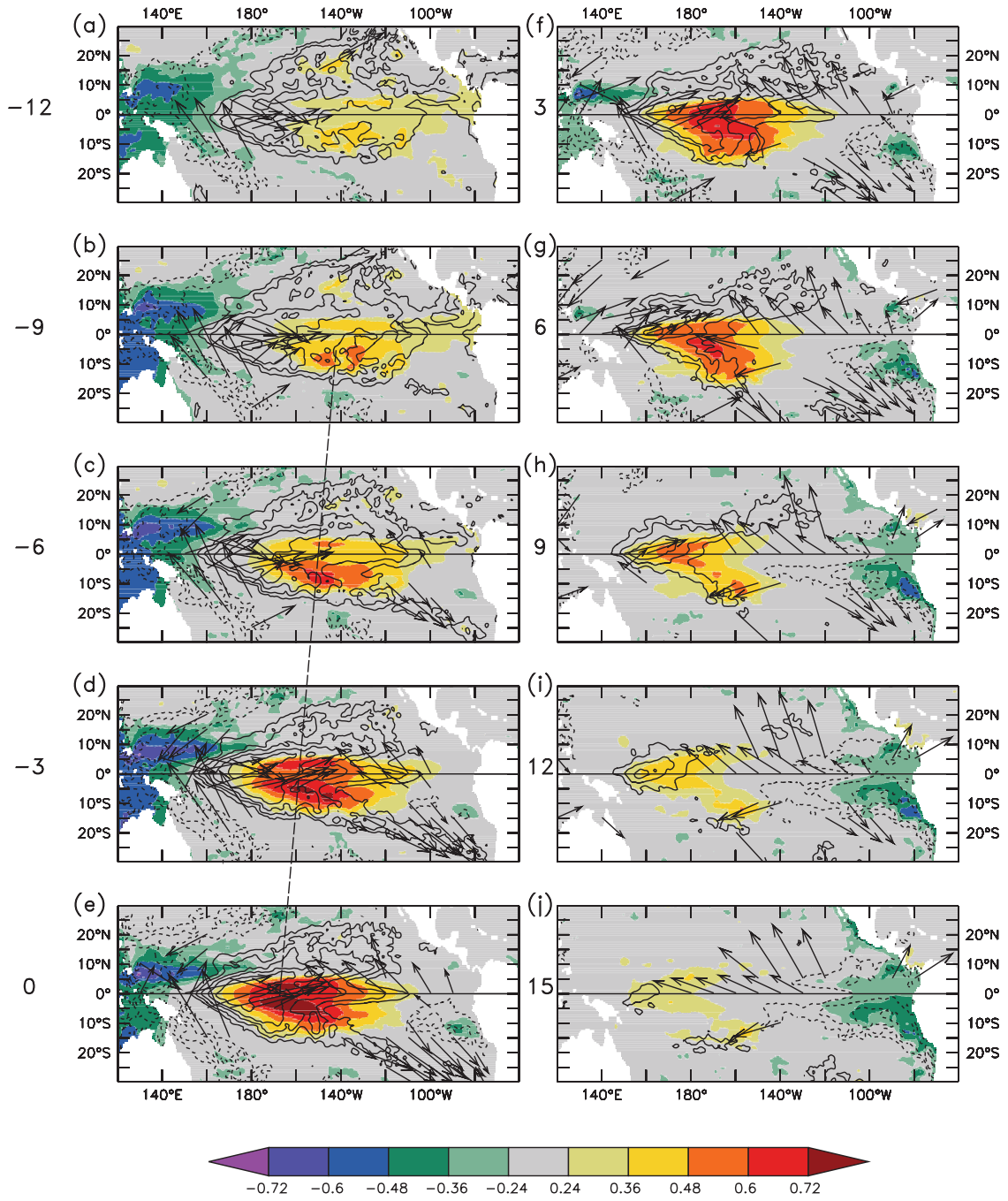

Figure 6. Lag/lead correlations of monthly EMI with sea surface height anomalies (shading) and ocean temperature anomalies at 10 m depth (contours). Positive (negative) correlation coefficients correspond to high (low) sea level anomalies. Regressed winds with EMI are shown only if the correlation coefficient between EMI and respective wind components exceeds 0.24. Significant correlations at a 80% (90%) confidence level are 0.24 (0.3) from a two-tailed Student's *t* test after taking into account the autocorrelations of EMI). The positive (negative) numbers to the left indicate the months by which the EMI leads (lags) the anomaly distribution fields. The thin line extending from Figures 6b to 6e indicates the propagation of off-equatorial Rossby waves.

Pacific, smear out the cold anomaly in the western Pacific. Thus the Modoki phenomenon is terminated (Figures 6f–6j, 7f–7j, and 8f–8j).

[28] The above picture demonstrates that the evolution of El Niño Modoki involves ocean-atmosphere coupled processes. Further, Figures 6–8 show a link of the El Niño Modoki with a distinct atmospheric component; the situation is analogous to the association of El Niño with the Southern Oscillation [*Bjerknes*, 1969; *Philander*, 1990]. Also, we have derived an atmospheric index by replacing

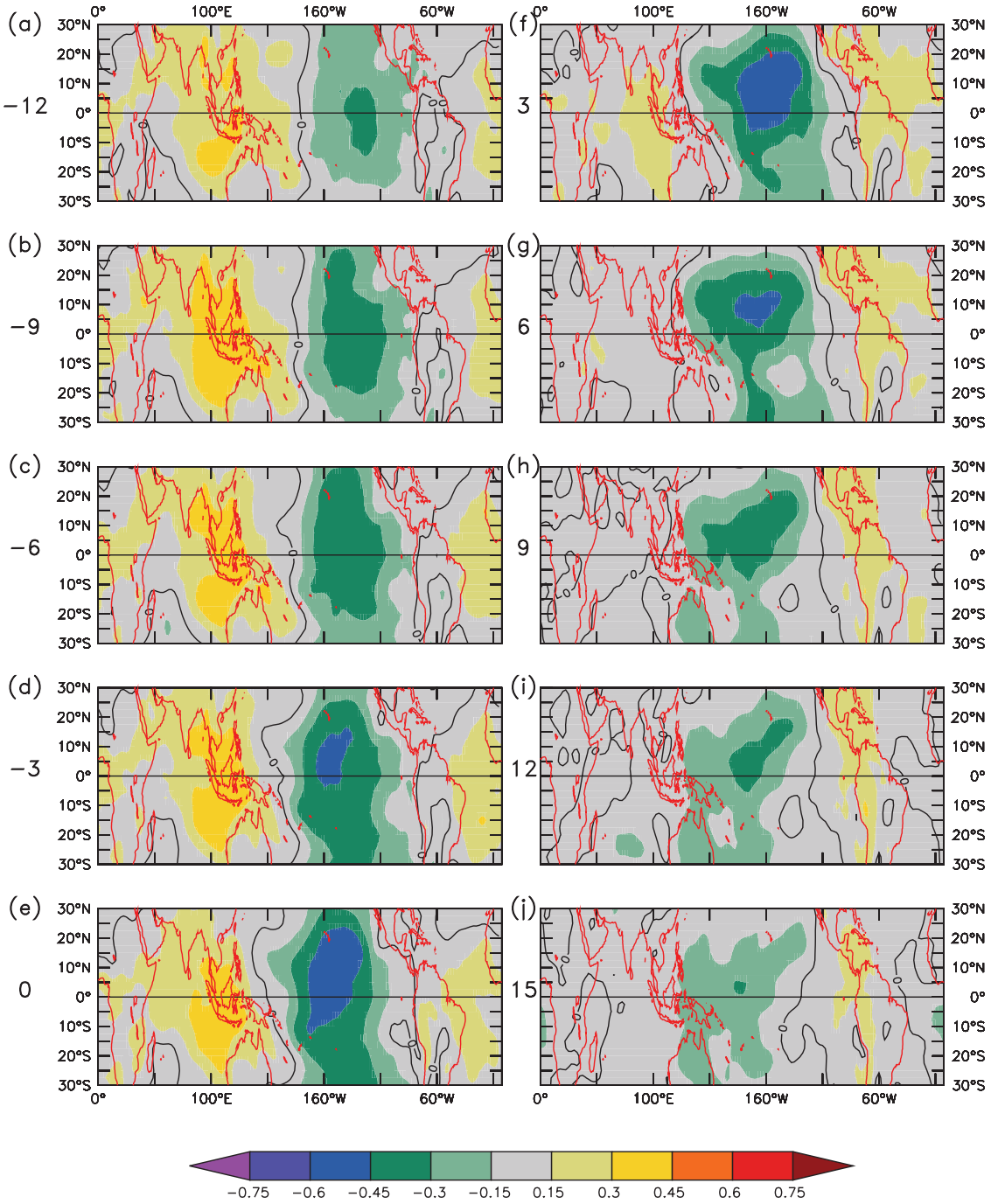

Figure 7. Lag/lead correlations of monthly EMI with sea level pressure anomalies. The positive (negative) numbers to the left indicate the months by which the EMI leads (lags) the anomaly distribution fields.

SSTA in the equation (1) with sea level pressure anomalies (SLPA), and reversed its sign (figure not shown). This atmospheric index has a significant correlation of 0.7 with EMI, demonstrating that there is a strong atmospheric response associated with the El Niño Modoki events. Thus the total entity should be referred to as ENSO Modoki.

[29] The tropical central Pacific is the common playground for both ENSO and ENSO Modoki. This is reflected in the lead/lag correlations between the indices of these phenomena, as discussed in section 3.1. It is important, however, to notice that the magnitude of these correlations is relatively modest. During the prominent El Niño events in years such as 1982–1983 and 1997–1998, the central Pacific warming propagates to the eastern Pacific. However, during majority of the El Niño Modoki events, the propagation takes place only up to the central Pacific.

[30] It is also important to notice that the ENSO Modoki timescales are different from ENSO. On the basis of a wavelet power spectrum analysis on EMI, we find (figure not shown), at a 90% significance level above red noise, (1)

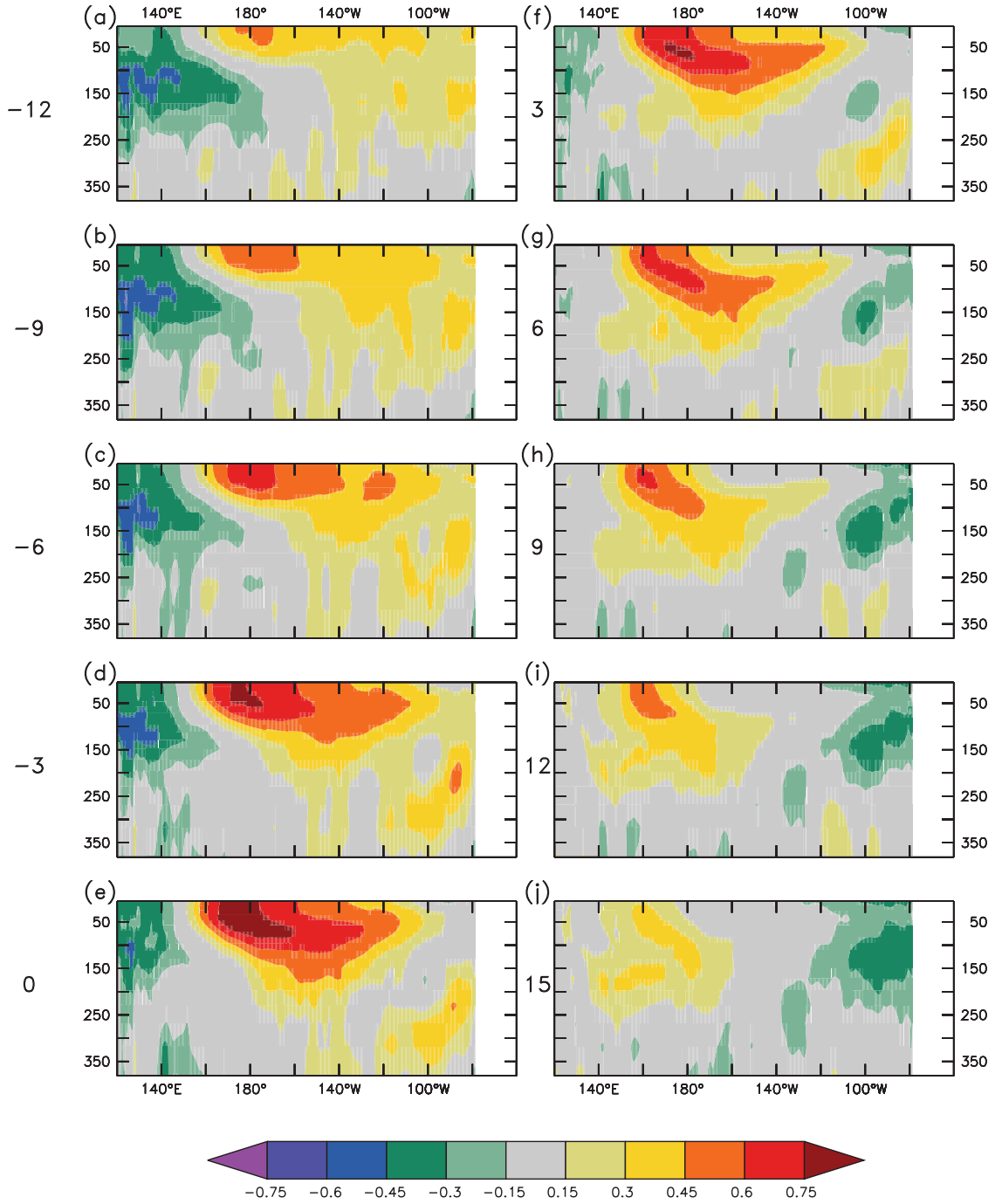

Figure 8. Lag/lead correlations of EMI with ocean subsurface temperature anomalies at different depths in meters averaged over 2°S–2°N. The positive (negative) numbers to the left indicate the months by which the EMI leads (lags) the anomaly distribution fields.

an interannual signal with 4-year periodicity and (2) a slowly varying signal with a 12-year timescale. The strong decadal signal modulating the interannual signal of EMI can be seen in Figure 4a. This strong decadal signature is unique to the EMI in the tropical Pacific; a similar wavelet power spectrum for NINO3 index for the period 1979–2004 does not exhibit any decadal peak significant at a 90% level above red noise. We note that the maximum monthly lead/lag correlations between the EMI and an index of the Pacific Decadal Oscillation [*Zhang et al.*, 1997; *Mantua et al.*, 1997] is about 0.4, indicating that a maximum of about 16% variance of either one of these phenomena is related to the other.

[31] The coupled processes discussed in this section apparently play a major role in setting up the interannual variability of the ENSO Modoki phenomenon. Further differences between the timescales of ENSO and ENSO Modoki are discussed by *Weng et al.* [2007].

[32] Preliminary examination of the lead/lag correlations of the SSHA with the statistically significant decadal signal

of EMI indicates some weak and slow wave propagation in the tropical and subtropical Pacific (figures not shown); this apparent propagation is different from that of similar correlations between the SSHA and the decadal signal of NINO3 SSTA, with the ENSO Modoki (ENSO) signal persisting largely in the tropical central (eastern) Pacific. However, this slow propagation may due to a statistical artifact. As our data span is only for 26 years, any interpretation of the decadal changes based on filtering has to be done with caution. The identification of a possible mechanism for the decadal variability of this phenomenon needs analyses of results from a high-resolution coupled model. This will be topic for future research.

3.4. Potential Impacts of the ENSO Modoki

[33] It is known that ENSO and Indian Ocean Dipole (IOD) generate atmospheric changes globally through teleconnections (see *Ropelewski and Halpert* [1987], *Aceituno* [1988], *Trenberth et al.* [1998], *Diaz et al.* [2001], *Saji and Yamagata* [2003], and *Yamagata et al.* [2004] for more details and further references]. For example, *Navarra et al.* [1999] tried to identify impacts of changes in the location of boreal summer peak warming in the tropical Pacific on the Indian summer monsoon. *Kidson et al.* [2002] discussed the different impacts of ''moderate'' and ''strong'' El Niños; their analyses, however, do not highlight the uniqueness of strong El Niño Modoki events. *Larkin and Harrison* [2005a, 2005b] have recently tried to study the autumn and winter impacts of the so-called ''dateline'' El Niño by composite analysis. Since their index is based on NINO3.4, their selection of years does not cover El Niño Modoki years 1979–1980, 1991, 1992, and 2002 (and also 2004, because their study is for the period 1950–2003).

[34] As the ENSO Modoki is associated with significant seasonal changes in the tropical SST and surface pressure changes, it is beneficial to study its potential impacts on the global climate by introducing seasonal stratification.

3.4.1. Boreal Summer Season

[35] Figure 9a shows the composite GPCP [*Adler et al.*, 2003] rainfall anomalies in the June–July–August–September (JJAS) season of the seven positive El Niño Modoki years 1986, 1990, 1991, 1992, 1994, 2002, and 2004. Statistically significant surplus rainfall anomalies are seen in the central equatorial Pacific region flanked on both sides by the negative rainfall anomalies in the equatorial western and eastern Pacific. The atmospheric condition associated with the western pole located in the equatorial western Pacific apparently influences maritime countries such as Indonesia, Malaysia, Singapore, etc., and the apparent teleconnection extends northwest up to south India and also Sri Lanka. The teleconnection associated with the positive rainfall anomaly in the central pole (equatorial central Pacific) seems to extend westward via the Philippines, Myanmar to northern India. In the east Asian region, southern Japan suffers droughts during these years owing to the Pacific-Japan pattern [see *Nitta*, 1987]. The deficit rainfall in the western Pacific region is seen to extend southward to southeastern Australia, influencing a significant part of eastern Australia. The negative rainfall anomalies over the equatorial eastern Pacific extend over western coast of North America.

[36] We adopt the partial correlation technique [e.g., *Pedhazur*, 1997; *Spiegel*, 1997; *Ashok et al.*, 2007] to isolate global impacts of the El Niño Modoki statistically from those of the ENSO and IOD during different seasons; this technique is equivalent to multiple regression (see Appendix B for details) In accord to the rationale of introducing the El Niño Modoki, the simultaneous linear correlation between the NINO3 index and EMI is very weak. Therefore the partial correlations of the EMI with seasonal rainfall and temperature anomalies are not influenced in almost all regions by the correlations with the NINO3 index (figures not shown). The correlation between the Indian Ocean Dipole Mode Index (IODMI) and EMI is also weak as we have already shown. However, during some years such as 1994, El Niño Modoki and positive IOD occur simultaneously and influence each other. The partial correlations of the EMI with the JJAS rainfall anomalies over the period 1979–2004, after removing the linear influence of NINO3 index and the IODMI, are shown in Figure 9b. The result is similar to that in Figure 9a. However, Figure 9b demonstrates the extensive influence of the ENSO Modoki on the eastern Australian region more clearly. The positive correlations from the central equatorial Pacific extend southeastward to southern regions of South America, indicating more than normal rainfall. The remarkable negative correlations in the eastern Pacific extend to the west coast of North America. This shows a dramatic contrast to the well-known impact of El Niño and is supported by an analysis using observed station data [*Weng et al.*, 2007]. We note that the negative correlations are also seen near Japan and south India. The robustness of the correlations has been reconfirmed by computing the significance levels based on a Monte Carlo method (Figure S1 in the auxiliary material).[1]

[37] It is expected that the impact of La Niña Modoki, with cooling in the central tropical Pacific flanked by warmer SSTA in eastern and western tropical Pacific, may be opposite to that of El Niño Modoki [*Diaz et al.*, 2001].

[38] Results obtained by repeating the composite analysis shown in Figure 9a with rainfall anomalies from CMAP data sets [*Xie and Arkin*, 1996] are qualitatively similar (figure not shown), though the magnitude of the significant composite anomalies is slightly different owing to the differences in the data sets [*Yin et al.*, 2004, and the references therein]. This exercise demonstrates the robustness of our results. Hereafter, all the subsequent precipitation analyses will be only based on the GPCP data sets.

[39] For comparison of the distinct impacts, the JJAS partial correlations between the NINO3 index and the rainfall anomalies over the period 1979–2004, with assuming the EMI and the IODMI as additional variables whose impacts have been removed, are presented in Figure 9c. In general, the results are in agreement with earlier studies (see *Diaz et al.* [2001] and *Saji and Yamagata* [2003] for details and further references). The eastern tropical Pacific receives surplus rainfall during El Niño years, with deficit rainfall in the tropical western Pacific and the equatorial South America. In contrast to the El Niño Modoki summers, northwestern America receives surplus rainfall. Over much of the South

[1] Auxiliary materials are available in the HTML. doi:10.1029/2006JC003798.

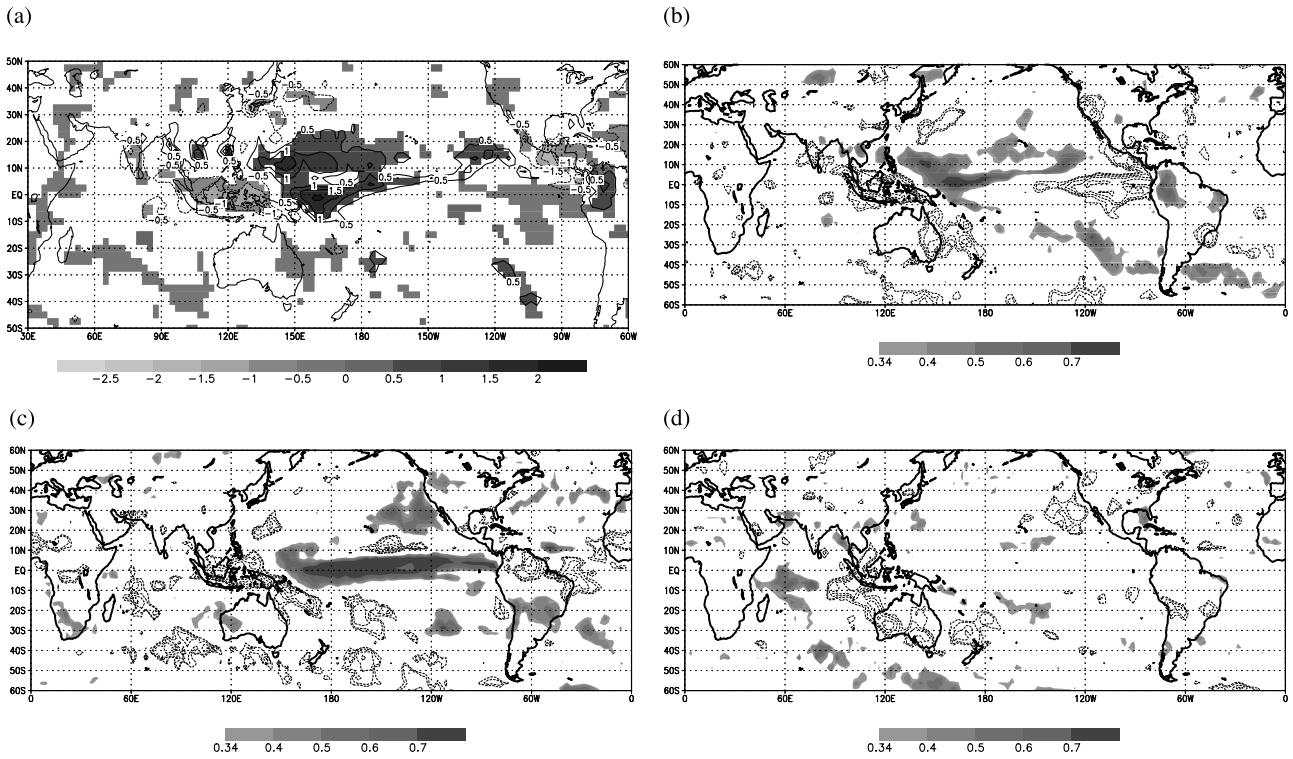

Figure 9. (a) Composite JJAS GPCP rainfall anomalies (cm/d) during strong positive El Niño Modoki events averaged over seven boreal summers, namely, JJAS seasons of 1986, 1990, 1991, 1992, 1994, 2002, and 2004. (b) JJAS (1979–2004) partial correlations of GPCP rainfall anomalies with EMI. Only significant values at 90% confidence level from a two-tailed Student's *t* test are shown; positive (negative) correlations are in shading (contours). The contours shown are −0.34, −0.4, −0.5, −0.6, and −0.7. See text for details. (c) Same as Figure 9b but with NINO3 index. (d) Same as Figure 9b but with IODMI.

American continent from equator to 40°S, the impacts of ENSO and those of ENSO Modoki are opposite. The impacts of ENSO on Australian winter rainfall have changed over the decades as found out by *Meyers et al.* [2007]. The El Niño events are apparently only associated with surplus rainfall in central western Australia during the study period. The impacts of the IOD on boreal summer rainfall derived by partial correlation analysis are presented in Figure 9d. In general, the impacts are similar to those shown in earlier studies [see *Saji and Yamagata*, 2003; *Ashok et al.*, 2003; *Yamagata et al.*, 2004; *Behera et al.*, 2005; *Rao and Behera*, 2005]. Positive IOD events cause anomalously deficit rainfall in Indonesia, more than two thirds of Australia, northern New Zealand, subtropical South America, parts of Mexico, North America, whereas surplus rainfall is seen in the region near the western pole of the IOD, Madagascar, parts of Africa, etc. The correlation is largely positive in northern India, though it falls just below the statistically significance level in the present analysis. This is in agreement with earlier studies showing IOD impacts on the Indian monsoon region [*Ashok et al.*, 2001; *Saji and Yamagata*, 2003; *Ashok et al.*, 2004]. Incidentally, we have repeated the multivariate analysis to assess the impacts of the IOD, ENSO, and ENSO Modoki by replacing the indices derived from HadISST with those from OISST for the available period (figures not shown). The correlations are qualitatively similar to those shown in Figures 9–11. However, with OISST indices, the positive (negative) correlations between the IODMI (NINO3 SSTA) and JJAS rainfall anomalies become statistically significant at 90% confidence level from a two-tailed Student's *t* test over a wide region of monsoon trough over India. Similarly, the negative IODMI-rainfall correlations become statistically significant over central Japan and Pakistan when we use the OISST data sets. However, even with SST data from *Reynolds et al.* [2002], the impact of ENSO events on India is seen to be limited and confined to eastern central India. In comparison, the impact from ENSO Modoki is seen over a larger area in southern India.

[40] In accord with the EOF analysis and composites of El Niño Modoki events, we find significant positive partial correlations between EMI and the surface air temperature anomalies over the central equatorial Pacific during boreal summer (Figure 10a). This positive correlation region apparently extends southeast; the positive correlations over Argentina and southern Brazil are significant, indicating that those regions experience warmer than normal winter during the El Niño Modoki event. Up north, significant cooling can be seen over northern Brazil, Columbia, and Venezuela, and parts of Mexico. Central and northern North America may also experience cooler summer during the El Niño Modoki years. Cooler than normal temperatures are also found around the maritime continent, in the tropical western Pacific, and in the southern part of China. These

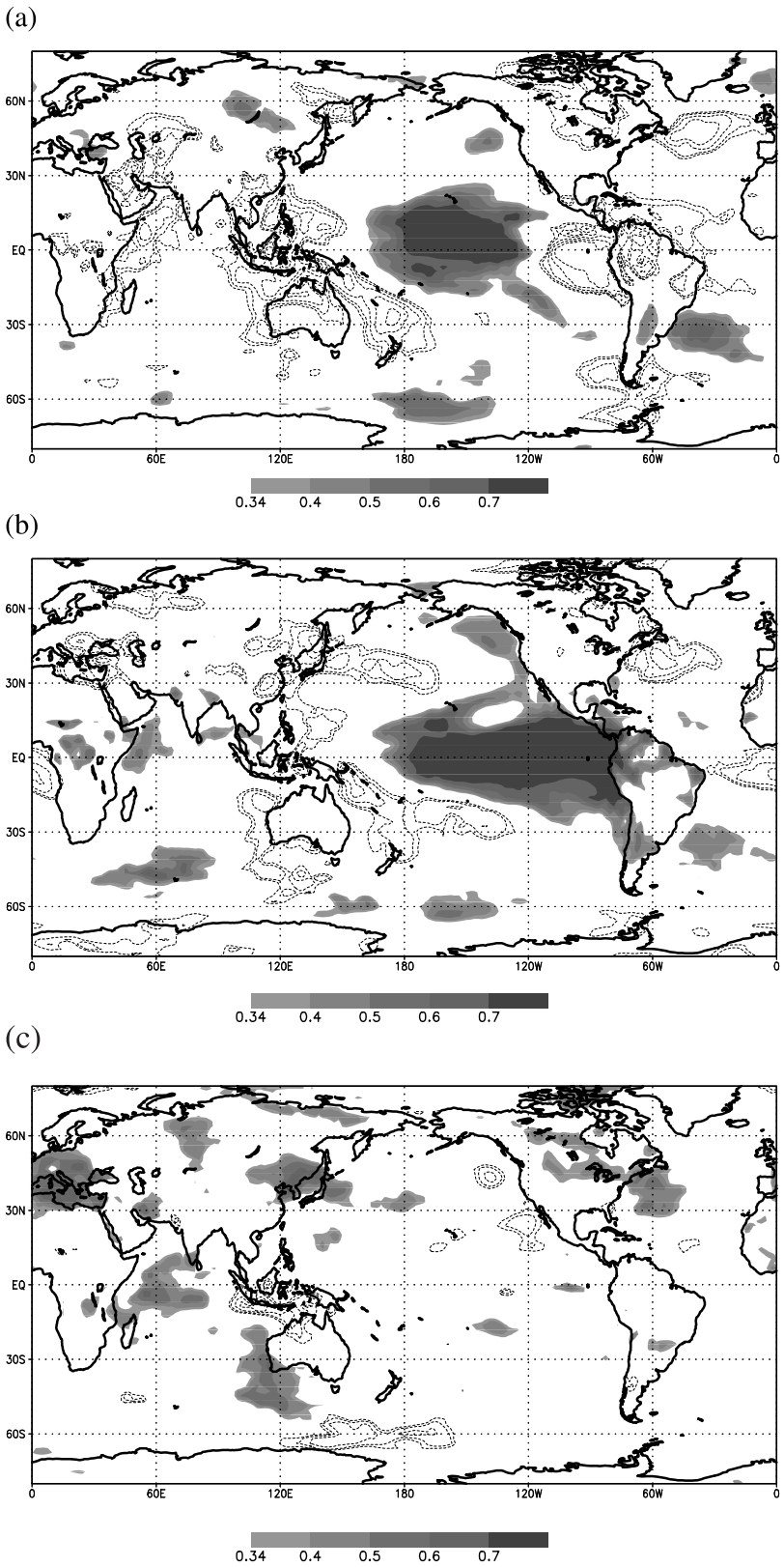

Figure 10. JJAS (1979–2004) partial correlations between temperature (2 m height) anomalies and (a) EMI (b) NINO3 index, and (c) IODMI. Only significant values at 90% confidence level from a two-tailed Student's *t* test are shown; positive (negative) correlations are in shading (contours). The contours shown are −0.34, −0.4, −0.5, −0.6, and −0.7.

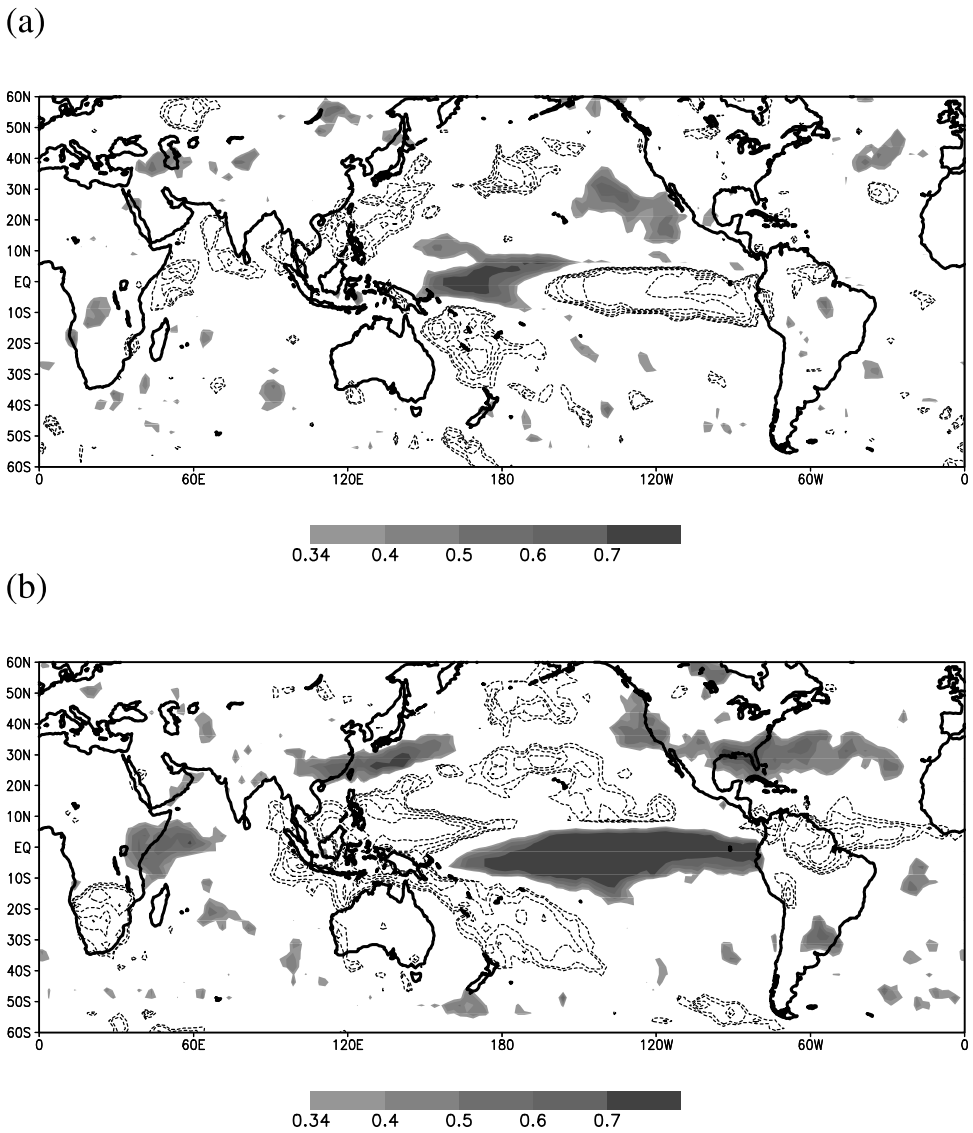

Figure 11. DJF (1979–2004) partial correlations between GPCP rainfall anomalies and EMI, significant at 90% confidence level from a two-tailed Student's *t* test; positive (negative) correlations are in shading (contours). The contours shown are −0.34, −0.4, −0.5, −0.6, and −0.7. (b) DJF (1979–2004) partial correlations between GPCP rainfall anomalies and NINO3 index.

significant negative partial correlations extend to western and northern Australia and New Zealand. Many of the regions along the east coast of Africa may experience anomalously cooler boreal summers during the positive El Niño Modoki events. A wide region in West Asia covering countries such as Turkmenistan, and Kazakhstan, Armenia, Georgia, etc., may also experience cooler than normal summer.

[41] To validate the NCEP/NCAR 2 m temperature data sets used in the above analysis, we have repeated the above analysis by replacing them with CRUTEM3 land temperature data sets [*Jones et al.*, 1999]. The results over the land regions are (figure not shown) qualitatively similar to those in Figure 10a, indicating that the NCEP/NCAR 2m temperature data sets over the study period can be reasonably used to understand the impacts of ENSO Modoki.

[42] The unique impacts of El Niño during boreal summer on anomalies of surface air temperature after removal of the effects of the ENSO Modoki and IOD are shown in Figure 10b. In North America, significant positive correlations can be seen along the Pacific coast up to Alaska. We also find similar warm anomalies along the Pacific coast in South America. In contrast, significant negative correlations are seen over the northeastern parts of US and Canada. Significant negative correlations can also be seen over the maritime continent, eastern China and Japan in east Asia, Turkey and southern Mediterranean Europe, indicating cooler summers during El Niño. In south Asia, significant positive correlations can be seen. Significant positive correlations are also seen over Central and East Africa. We see that the impacts of the ENSO are opposite to those of ENSO Modoki over many regions such as tropical South America,

equatorial Africa, and India. This again confirms that the ENSO Modoki is different from ENSO.

[43] For completeness, we show the partial correlations between the IODMI and JJAS surface temperature in Figure 10c. Besides the familiar dipolar structure over the tropical Indian Ocean, correlations indicate that the positive IOD events cool the maritime region and north central Australia significantly during austral winters. In contrast to the El Niño influence, southwest Australia significantly warms up during positive IOD events. Many regions in the Northern Hemisphere such as the Far East including Japan, the Mediterranean and Europe, US and central Canada experience warmer summer when a positive IOD event occurs, in confirmation of earlier studies [*Saji and Yamagata*, 2003; *Guan and Yamagata*, 2003; *Yamagata et al.*, 2004].

3.4.2. Boreal Winter Season

[44] The boreal winter (DJF) partial correlations of the EMI with the rainfall anomalies over the period 1979–2004, after removing the linear influence of NINO3 index, are presented in Figure 11a. Their robustness is verified in Figure S2 in the auxiliary material by the Monte Carlo method; the IOD events, in general, terminate by the end of November because of their strong seasonally phase-locked life cycle due to reversal of monsoonal winds over the equatorial Indian Ocean [*Saji et al.*, 1999; *Rao and Yamagata*, 2004; *Rao et al.*, 2007], and hence the IOD influence is removed almost automatically. The equatorial eastern Pacific receives less than normal rainfall when El Niño Modoki is active. The positive partial correlations in the central equatorial region extend northeastward to Mexico. Some parts of the maritime countries, southern Thailand, the Philippines, southern India, Sri Lanka, and East Africa experience anomalous dry conditions. On the other hand, significantly wet conditions are seen over New Zealand, Pakistan, Kazakhstan, and parts of south central Africa.

[45] During El Niño events, as seen in Figure 11b, a wide area in the western Pacific region extending from the Philippines to Western Australia through the maritime continent experiences deficit rainfall. On the other hand, another wide region from the central to eastern equatorial Pacific receives above normal rainfall, which is very different from the impacts of El Niño Modoki. The southern part of the African continent, equatorial South America and northern New Zealand in the Southern Hemisphere experience drier summer during El Niño, whereas regions of northern Argentina, southeast Brazil and Uruguay experience wetter summer. Significant wet conditions are also seen from northeast Africa to central India and further to Far East through southern China. We also note that North America receives above normal rainfall.

[46] The most prominent impact of EMI events on surface temperature during boreal winter is, as expected, the warming over the central equatorial ocean and the cooling on both sides, i.e., over the eastern equatorial Pacific and over the maritime continent including the Philippines in Northern Hemisphere, and western and southern Australia in the Southern Hemisphere (Figure 12a). The west coast of Mexico may experience warmer winter. On the other hand, El Niño Modoki events appear to cause anomalously cold winters in eastern India and eastern Europe. The subtropical east coast of South America also has cooler than normal austral summer.

[47] El Niño impacts on boreal winter surface temperature seem to be more extensive and different from the El Niño Modoki impacts as seen in Figure 12b [see also *Yamagata and Masumoto*, 1992]. Except for the western tropical Pacific, the global tropical region in general is warmer during El Niño winters [see *Pan and Oort*, 1983]. This is particularly pronounced in the tropical Indian Ocean through changes of Walker circulation [see *Yamagata et al.*, 2004]. El Niño also brings warmer than normal boreal winters over the west coast of Mexico and United States and along a zonal belt across the northern North America. Western inland Mexico is cooler during the same period. The region from the South China Sea to Japan is warmer than normal during El Niño winters. The eastern and southwestern Australian region is warmer than normal, whereas New Zealand is colder than normal. Those impacts of El Niño are, in general, similar to earlier studies [e.g., *Diaz et al.*, 2001; *Saji and Yamagata*, 2003].

3.4.3. Possible Teleconnection Mechanisms

[48] To understand possible mechanisms of the teleconnection pattern of the ENSO Modoki phenomenon, we have computed the JJAS partial correlations between the EMI and global SLPA after removing the influence of ENSO and IOD phenomena (Figure 13a). A large area in the central Pacific is covered by negative correlations that indicate anomalous depression of surface pressure during El Niño Modoki summers; the rest of tropical regions are covered by positive correlations indicating anomalous high-pressure areas sandwiching the low-pressure area in the center. The central negative correlations extend west toward northeast India via the Philippines and toward 120°E through New Zealand in the Southern Hemisphere. The composite distribution of JJAS SLPA in summers of strong El Niño Modoki (figure not shown) is in agreement with Figure 13a. A similar composite distribution of the anomalous circulation at 850 hPa shows the central Pacific convergence of anomalous westerlies in the western equatorial Pacific and anomalous easterlies in the eastern equatorial Pacific (Figure 13b). The composite wind anomalies at 200 hPa over the tropical Pacific are opposite in sign in the same region (Figure 13c), indicating the presence of two anomalous Walker circulation cells in the troposphere. The joint ascending branch of these cells is located in the central equatorial Pacific. This double cell pattern shows a marked difference from the single cell pattern in the typical El Niño case. It is clearly seen when an El Niño Modoki event occurs during boreal winters, such as in DJF 2004/2005 (Figure 14). The anomalous circulation in the tropical zonal-vertical plane is consistent with the surplus rainfall in the ascending region of the central tropical Pacific and the deficit rainfall in the descending regions. The precipitation anomaly distribution (Figures 9a and 9b) is basically consistent with the SLPA correlations (Figure 13a).

[49] The impacts of the ENSO Modoki on the climate of the surrounding subtropical region may be attributed to the Rossby wave train generated by the diabatic heating in the central tropical Pacific [see *Wang et al.*, 2003; *Saji et al.*, 2005]. Another relevant hypothesis is given by *Trenberth et al.* [1998], who suggest that the Hadley circulation due to the tropical forcing induces changes in convergence/divergence patterns in subtropics that in turn act as Rossby wave source, subject to some constraints such as the location of

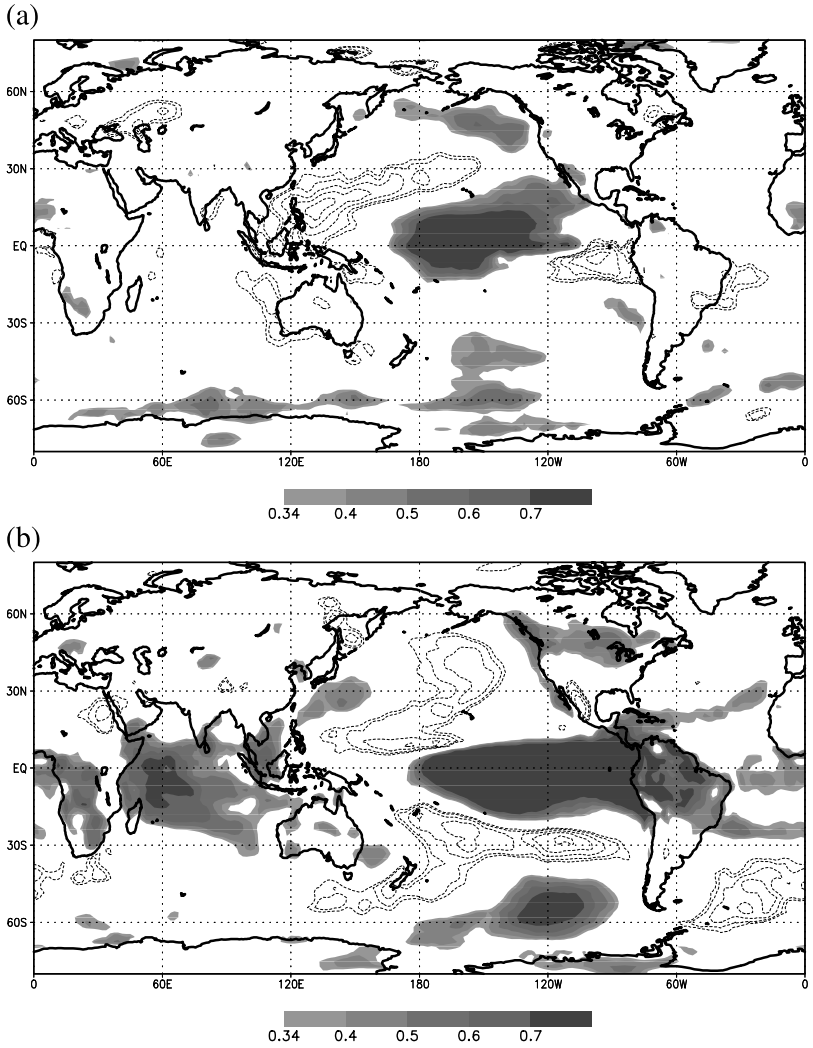

Figure 12. (a) Same as Figure 10a but for DJF season. (b) Same as Figure 10b but for DJF season.

heat source, interaction with the climatological stationary planetary waves.

[50] As seen in Figures 13b and 13c, it is inferred that the atmospheric response to the El Niño Modoki is baroclinic in the tropics, whereas it has an equivalent barotropic structure in the subtropics. The basic mean state of midlatitude atmospheric circulation plays an important role in transmitting the energy from the tropics to midlatitudes [*Hoskins and Karoly*, 1981; *Trenberth et al.*, 1998; *Diaz et al.*, 2001; *Kidson et al.*, 2002]. The JJAS partial correlations of the EMI with geopotential anomalies at 500 hPa are shown in Figure 15a. The response is unipolar in the tropics and subtropics, and wave trains can be seen in midlatitudes of Northern Hemisphere. The response in the Southern Hemisphere appears to be a wave number 1 pattern. The DJF partial correlations between EMI and geopotential anomalies at 500 hPa (Figure 15b) indicate stronger response in the Northern Hemisphere. The stronger teleconnections in the winter hemisphere may be due to the phase locking of the stronger subtropical and subpolar jet streams that act as waveguides in carrying the energy from tropical heat sources [e.g., *Hoskins and Karoly*, 1981; *Webster*, 1982; *Diaz et al.*, 2001; *Wang et al.*, 2003; *Saji et al.*, 2005]. Also, the modulation of the jet stream intensity and location by the ENSO Modoki events, just as by the ENSO and IOD events [*Nakamura and Shimpo*, 2004; *Ashok et al.*, 2007], may induce teleconnections in higher latitudes.

[51] Another process through which the ENSO Modoki events may influence the east Asian region is possibly through a combination of two mechanisms, namely, the monsoon-desert mechanism [*Rodwell and Hoskins*, 1996] and the Silk Road pattern [*Enomoto et al.*, 2003]. (The Indian monsoon is influenced by the tropical SSTA forcing during ENSO and IOD events. *Rodwell and Hoskins* [1996] suggested that the changes in Indian monsoon affect the Mediterranean/Sahel region through the long Rossby wave response, a process that is now known as monsoon-desert mechanism. While examining the evolution of the summer condition over Japan region, *Enomoto et al.* [2003] suggest that as the Asian jet acts as a waveguide to transmit the impact from Mediterranean region all the way up to east Asia. This process has been named the Silk Road pattern. Several publications [*Guan and Yamagata*, 2003; *Saji and Yamagata*, 2003] indicate that the impacts IOD during boreal summer are carried to east Asian/Japan region by a combination of these mechanisms. We hypothesize that

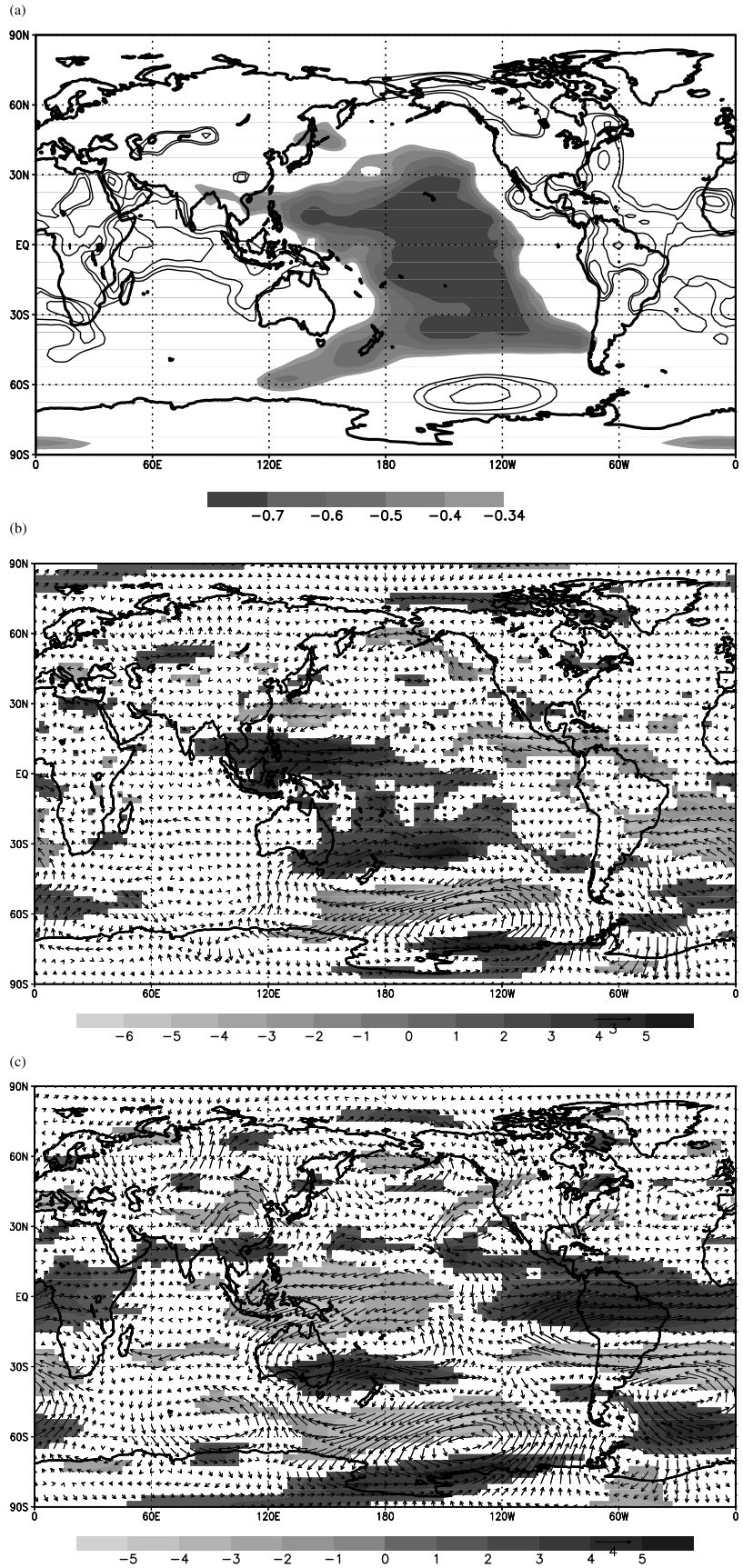
(a)
90N
60N
30N
EQ
30S
60S
90S
0
60E
120E
180
120W
60W
0
−0.7 −0.6 −0.5 −0.4 −0.34
(b)
90N
60N
30N
EQ
30S
60S
90S
0
60E
120E
180
120W
60W
0
−6 −5 −4 −3 −2 −1 0 1 2 3 4 5
(c)
90N
60N
30N
EQ
30S
60S
90S
0
60E
120E
180
120W
60W
0
−5 −4 −3 −2 −1 0 1 2 3 4 5

Figure 13

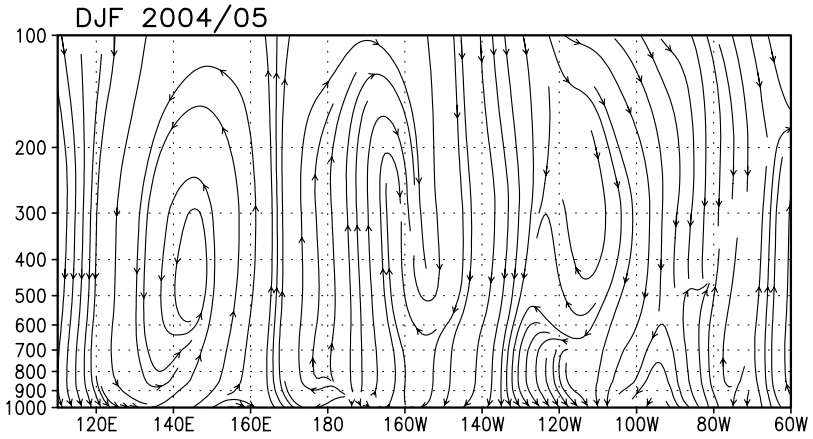

Figure 14. The 2004–2005 DJF anomalous Walker circulation streamlines averaged from 10°S to 10°N.

these mechanisms also may act during the El Niño Modoki events and thereby transmit their impacts to higher latitudes in the Northern Hemisphere.) The other, not alternative, way in which the ENSO Modoki may influence the east Asia, in particular, Japan, is through a mechanism analogous to the one proposed by *Nitta* [1987], which is popularly known as the Pacific-Japan (PJ) pattern. (According to *Nitta* [1987], the SST in the tropical western Pacific (10°N–20°N, 150°E–170°E) are anomalously colder during a typical El Niño event. The convection is inactive over the Philippine Sea during such years. This induces an anomalous response further north, causing cool and wet summers over Japan. During the typical La Niña years, in contrast, the SST anomalies are opposite over the aforementioned region, and consequently, impact over the east Asia is the opposite.) This mechanism essentially involves a modulation of the tropical-subtropical Hadley circulation due to changes in the tropical SST. It is interesting to note that significantly drier and warmer conditions are seen over Japan during El Niño Modoki events; this impact is just opposite to that of El Niño events (Figures 9 and 10).

[52] Though further details of the ENSO Modoki teleconnection mechanism have to be worked out, the fact that impacts of the ENSO Modoki are quite different from those of ENSO in many regions over the globe supports the uniqueness of the El Niño Modoki phenomenon.

4. Modulation of ENSO Modoki: Possible Links to Background Changes

[53] The EOF2 pattern obtained from an EOF analysis of the tropical Pacific SSTA over the domain shown in Figure 2a but for the period of 1958–1978 (Figure 16) does not show any clear maximum variance in the central tropical Pacific; actually, it looks more like an ENSO (compare Figures 2a and 2b). The ENSO Modoki is also not represented by the next two higher modes for this period. The maximum lead correlation of the PC1 with PC2 for this period, occurring at a lag of 10 months, is −0.6, indicating that about 36% of variability of EOF2 is related to ENSO, unlike for the period after 1978.

[54] A similar EOF analysis of SSTA from an extended period from 1958 through 2004 indicates that the ENSO Modoki pattern appears as EOF3, explaining about 9% of the variance (figure not shown). We find that the ENSO Modoki events that have been identified in the present study based on EMI are also well represented by the PC3 from the extended period EOF analyses. The events prior to 1979 were relatively weak and short-lived, and hence the relatively low variance explained the EOF3; A hint of this is also obtained from similar EOF analyses by *Meyers et al.* [1999] based on the data sets from 1868–1993. This indicates that increase in the ENSO Modoki events after 1979 has enhanced their role in tropical Pacific variability.

[55] These analyses confirm that ENSO Modoki is relatively dominant in the tropics after 1978 as compared to the earlier period, and that a large portion of ENSO Modoki variability is not associated with the ENSO phenomenon since 1979. The occurrence and life period of the ENSO Modoki events have increased since the early 1980s, and hence the ENSO Modoki events appear as one of the top two dominant modes of the tropical Pacific SST variability, each of which seems to be associated with its own distinct nature of tropical coupled dynamics. It will be interesting to discuss possible reasons for the recent increase in variance explained by such a higher coupled mode. Figure 17a shows the long-term change in mean SST, obtained by subtracting the mean SST for the period 1958–1978 from that for the period 1979–2004. This difference distribution, which can be interpreted as either a long-term trend or an interdecadal

Figure 13. (a) JJAS (1979–2004) partial correlations between SLPA and EMI. Shaded values are significant at 90% confidence level from a two-tailed Student's *t* test; negative (positive) correlations are in shading (contours). The contours shown are 0.34, 0.4, 0.5, 0.6, and 0.7. (b) Composite JJAS 850 hPa anomalous winds obtained from seven strong El Niño Modoki events. Shaded reasons indicate zonal winds significant at 90% confidence level from a two-tailed Student's *t* test. (c) Same as Figure 13b but at 200 hPa level.

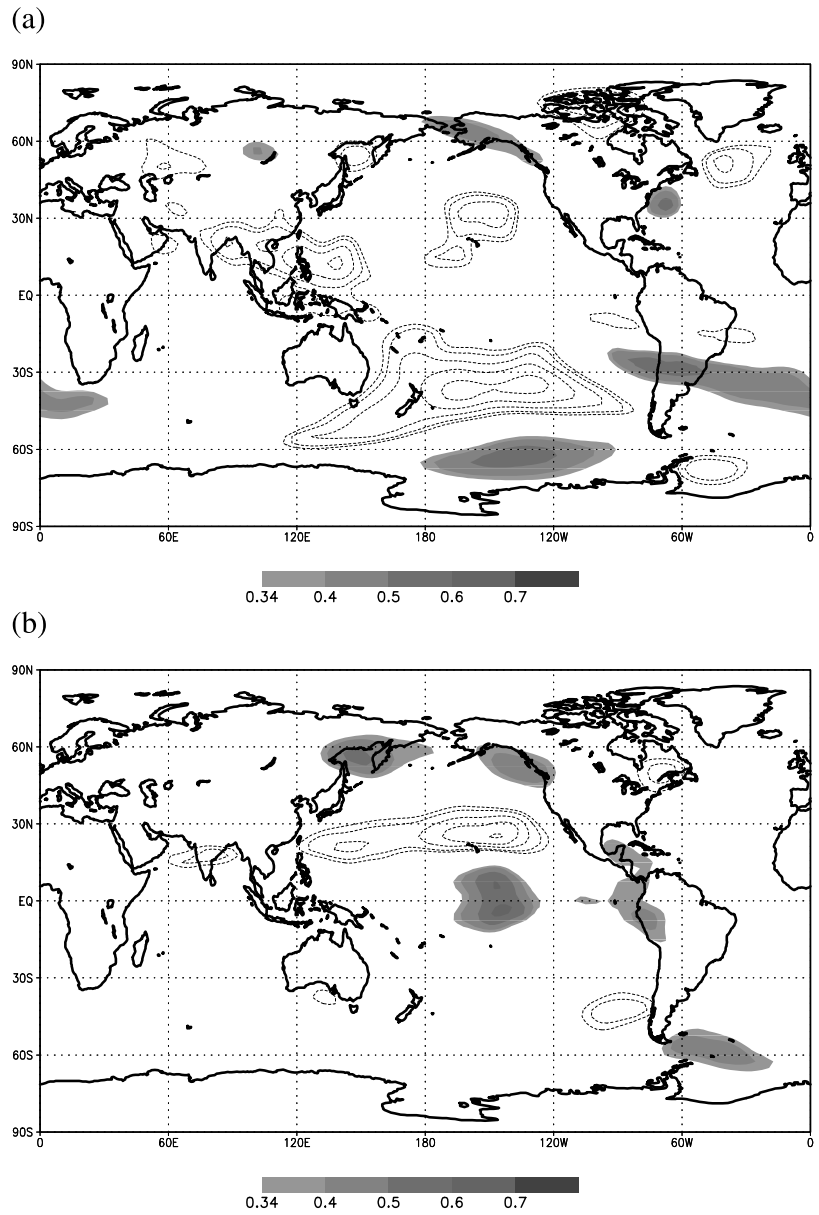

Figure 15. (a) JJAS (1979–2004) partial correlations between 500 hPa geopotential anomalies and EMI. Significant values at 90% confidence level from a two-tailed Student's *t* test are shown; negative (positive) correlations are in shading (contours). The contours shown are 0.34, 0.4, 0.5, 0.6, and 0.7. (b) Same as Figure 15b but during DJF (1979–2004).

change, shows general warming over most of the globe between 60°S and 60°N except for the northern North Pacific where there is significant cooling as described by the *Intergovernmental Panel on Climate Control* [2001], *Deser et al.* [2004], and *Hartmann and Wendler* [2005]. Interestingly, maximum SST warming regions in the tropical Pacific are located just off the equator in the eastern Pacific. We have also verified that the annual SST climatology difference is in agreement with the heat content changes at 300 m depth (figure not shown). This sort of SST trend in the equatorial Pacific is associated with the low-level wind trend (Figure 17a). We see that most of the area of the tropical Pacific is dominated by enhanced westerly anomalies, indicating that equatorial easterly winds have weakened as discussed by *Inoue and O'Brien* [1987], *Kitamura* [1990], and *Yamagata and Masumoto* [1992, Figure 17b]; we further confirm the weakening of the low-level easterly winds by a similar analysis (figure not shown) based on ERA-40 data sets [*Simmons and Gibson*, 2000]. The weakened easterlies over the equatorial central Pacific and enhanced easterlies in the eastern Pacific weaken the zonal gradient of SST as well as the zonal tilt of the thermocline. The relative flattening of the thermocline in the recent period can be seen by calculating the difference of isotherms in two different periods (Figure 17c). This finding is in agreement with the ocean temperature trend in the equatorial Pacific for the period 1945–1993, as shown in an earlier study [e.g., *Liu and Huang*, 2000, Figure 2a]. The

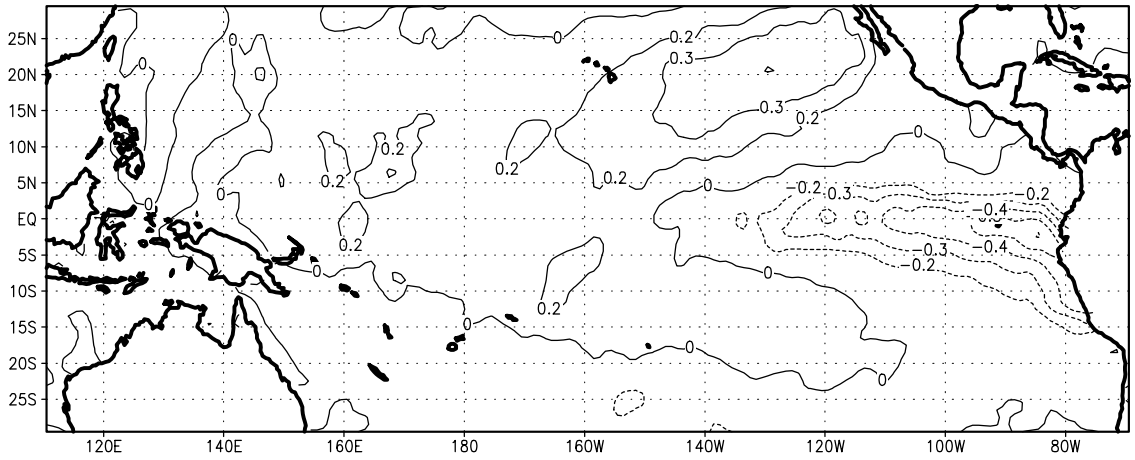

Figure 16. EOF2 mode of tropical Pacific SSTA (1958–1978) multiplied by its standard deviations of the principal component; units in °C. This mode explains about 10% of the tropical Pacific SSTA variance.

change related to weakening of low-level easterlies in the central equatorial Pacific reflects the present climate state that favors the formation of more El Niños as compared to La Niñas [e.g., *Namias et al.*, 1988; *Nitta and Yamada*, 1989; *Fedorov and Philander*, 2000; *Philander*, 2004]. This also means that the present-day climate is less conducive to turnabout of ENSO events as compared to the period of 1960–1978. Another way to describe this trend is to introduce a concept of El Niño-like decadal phenomenon [*Luo and Yamagata*, 2001; *Annamalai et al.*, 2005; *Lohmann and Latif*, 2005]. However, we here suggest that such a trend may be attributed to the recent frequent occurrence of the ENSO Modoki event.

[56] The EOF3 structure shown in Figure 2c and its associated principal component PC3 shown in Figure 3 provide potential clues to interpret the recent decadal changes in ENSO Modoki occurrence in terms of background changes. It is interesting that the PC3 exhibits a long-term increasing trend since 1979. It is also seen that after 2001, the PC3 was in such a phase that strengthens the SSTA gradient between the central tropical Pacific and eastern tropical Pacific, there by increasing the El Niño Modoki condition. The magnitude of the correlation between PC2 and PC3 for the period 1998–2004 increased to 0.71, showing that the modes were in tandem during this period. This has some implications for the strength of ENSO Modoki. For example, the major contribution to the tropical Pacific summer SSTA in 2004 is from EOF2 (figure not shown). This structure is enhanced in the central and eastern tropical Pacific by contribution from EOF3 (figure not shown). The long-term phase of the PC3 has changed around 1987–1988, and this appears to be associated with a further increase in ENSO Modoki frequency thereafter.

5. Summary and Discussion

[57] We have identified a new tropical Pacific ocean-atmosphere coupled phenomenon that is named as El Niño Modoki (pseudo-El Niño) in this article. A typical example of a positive phase of this phenomenon is found in 2004, with warming in the central tropical Pacific, flanked by anomalously colder than normal SSTA in the western and eastern Pacific. The event is different from the conventional ENSO event. An EOF analysis performed on the monthly SSTA from 1979 to 2004 shows that the El Niño Modoki is similar to the EOF2 pattern that explains about 12% of the tropical Pacific SST variability.

[58] Using a composite analysis method, we have demonstrated the physical existence of El Niño Modoki and its unique impact on the world climate. The composite and correlation analyses of SSH, SST, ocean subsurface temperature SLP, and zonal wind anomalies indicate that the El Niño Modoki is an ocean-atmosphere coupled phenomenon which is distinct from El Niño. The central SST warming and associated zonal wind convergence on either side of the SSTA sustain the event for almost a year. Interestingly, the coupled mode appears almost as a standing mode in the central Pacific, and does not evolve into a full-fledged El Niño event. The partial correlation analysis identifies many regions over the world where the temperature and rainfall are significantly influenced by the ENSO Modoki phenomenon during boreal summer as well as boreal winter. In the tropics, this extensive impact is due to anomalous twin Walker circulation cells with their common updraft branch centered over the central tropical Pacific pole of the SSTA tripole of ENSO Modoki. The impacts are transmitted to higher latitudes as in the cases of ENSO and IOD. The impacts propagate into the winter hemisphere more efficiently because of relatively stronger seasonal subtropical and subpolar jet streams, which is in agreement with many past studies related to ENSO teleconnection.

[59] Because of its double cell structure in the atmosphere in accord to the tripole structure in SSTA, the ENSO Modoki may be classified as a higher coupled mode compared to the gravest ENSO mode. The present study also shows that most of the ENSO Modoki events during the study period are not a part of ENSO evolution. The background state during the present warm climate appears to be relatively less conducive to the turnabout of ENSO events in comparison with the period 1958–1978; it appears more conducive to rather persistent occurrence of the ENSO

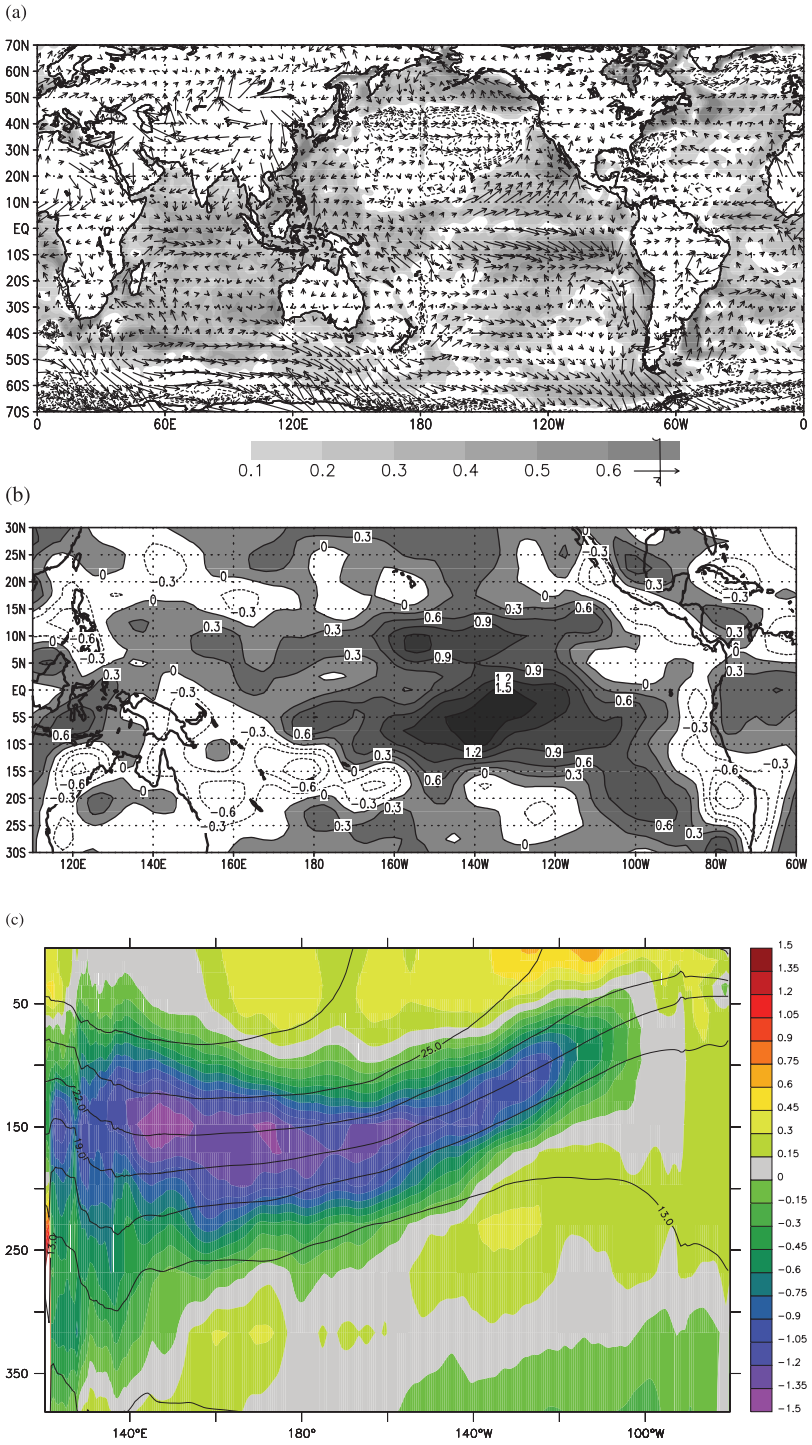

Figure 17. (a) Long-term changes in mean SST (°C) and winds at 1000 hPa (m/s), obtained by subtracting the mean SST of the period 1958–1978 from that over the period 1979–2004. (b) Long-term changes in annual mean zonal winds at 1000 hPa (m/s), obtained similar as to Figure 17a. (c) Differences of ocean temperature in two periods of 1958–1978 and 1979–2004 along with the depth-longitude section of climatological ocean temperature (black contours).

Modoki. A recent study by *Monahan and Dai* [2004] suggests that the temporal and spatial nonlinear relationship of the first two modes of the tropical Pacific SST variability leads to the nonlinear structures of El Niño and La Niña. This nonlinear relationship may also be subject to the changes in the background conditions. Also, there is certainly asymmetry in the strengths of El Niño and La Niña in real world. This asymmetry [*Rodgers et al.*, 2004; *An and Jin*, 2004] per se, however, cannot result in ENSO Modoki owing to the reason that both El Niño and La Niña do not

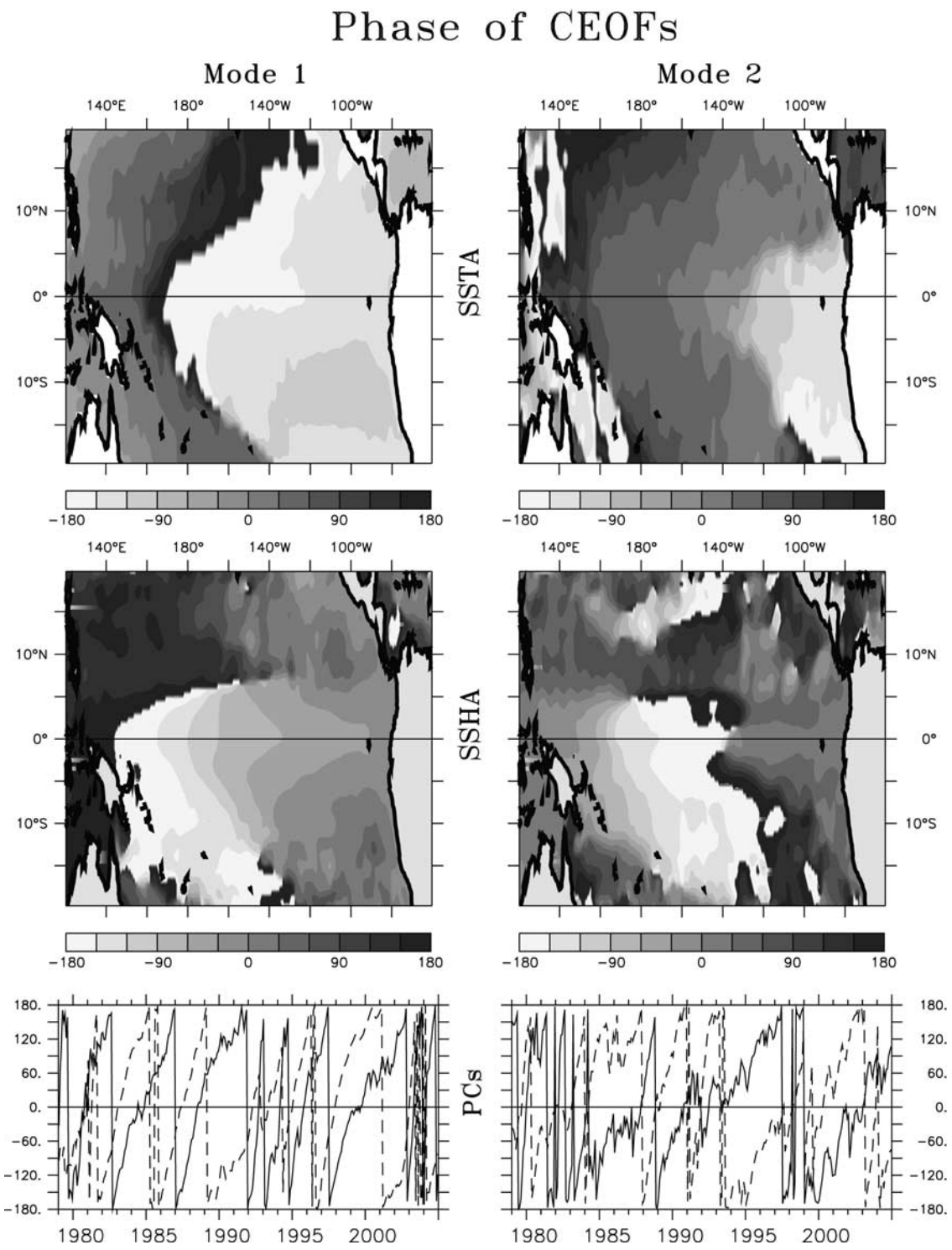

Figure A1. The phase information of (top left) complex EOF1 and (top right) complex EOF2 of SSTA. (middle) Similar information for SSHA. (bottom) Respective principal components, with thick (dashed) lines representing the SSTA (SSHA).

occur simultaneously. However, a very strong El Niño can leave some residual signal. This residual, in turn, can interact with a following La Niña and manifest as a Modoki; this sort of scenario can be interpreted as a change in background conditions. Yet, it should also be noted that Modoki events such as 2004 have no preceding strong signals of ENSO, as already discussed.

[60] We suggest that ENSO and ENSO Modoki comprise two major orthogonal modes of the ocean-atmosphere coupled system in the tropical Pacific. On the basis of the background state, the Pacific coupled system may prefer

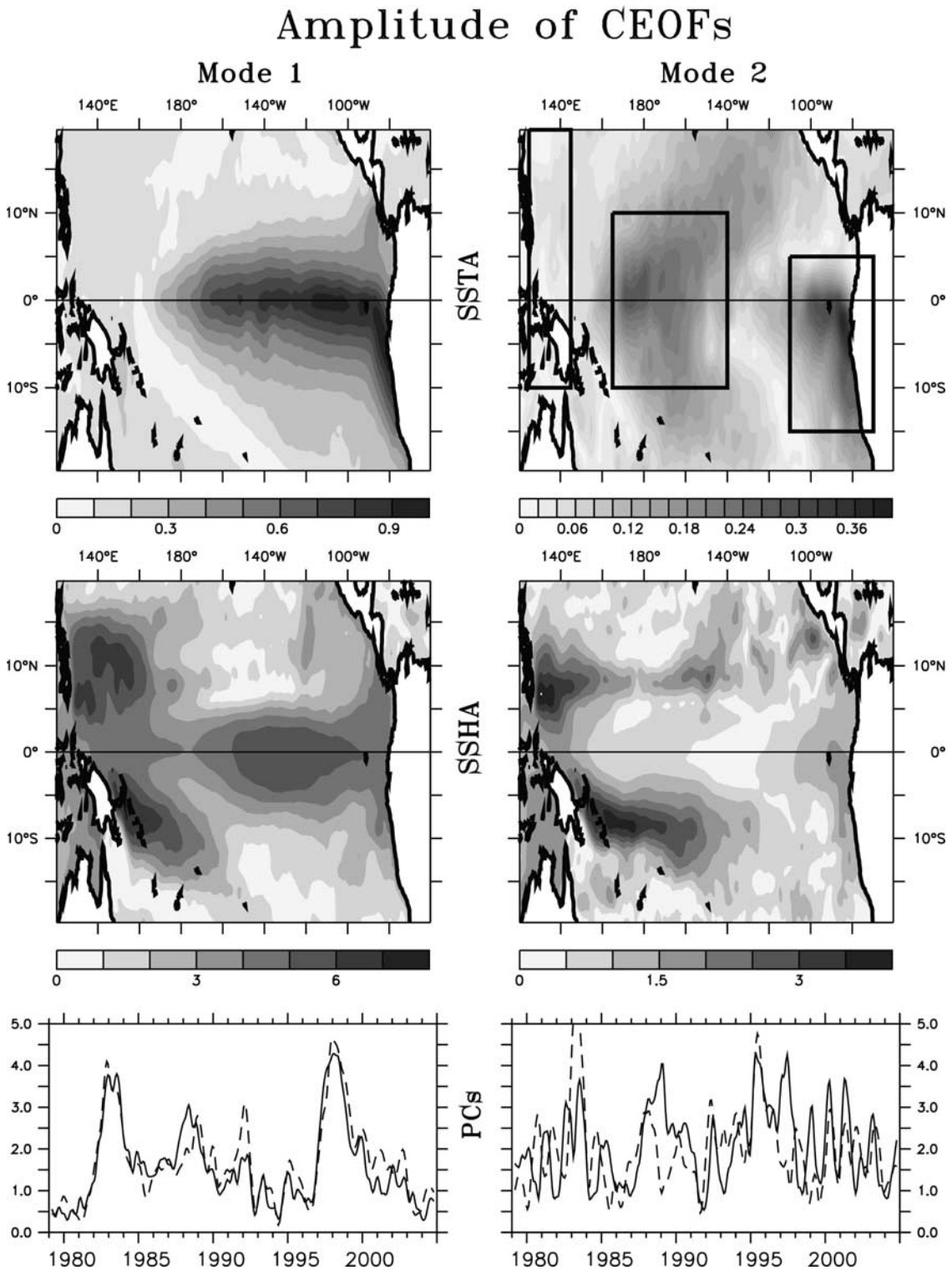

Figure A2. The amplitude of (top left) complex EOF1 and (top right) complex EOF2 of SSTA. (middle) Similar information for SSHA. (bottom) Respective principal components, with thick lines representing the SSTA and dashed lines for SSHA.

one of these dominant coupled modes. Rather than referring to ENSO Modoki as a part of ENSO by changing the definition of ENSO, we have proposed another way to view the recent climate conditions in the tropical Pacific from a new angle.

[61] There are several aspects that need further investigation about the ENSO Modoki introduced in the present paper. Its teleconnection needs to be studied in more detail using observational data and coupled models. Also, most of the processes discussed here are subject to severe limitation

of a linearized view. Nevertheless, the ENSO Modoki, just like other climate element modes such as ENSO and IOD, appears to be important in deepening our understanding of global climate variability. The reason why the ENSO Modoki occurs more frequently and persistently in recent decades also needs thorough investigation from a viewpoint of the global warming trend. Another interesting direction of research is to examine the potential role of intraseasonal wind bursts [*McPhaden*, 2004] which may trigger these climate modes in a different way under different background conditions by influencing the propagation of the coupled downwelling Kelvin waves (K. Ashok et al., manuscript in preparation, 2007). Considering the increasing importance of the ENSO Modoki event in the recent tropical Pacific variability, attempts to predict the phenomenon should also be started; this will lead to better seasonal prediction, and certainly benefit our society.

Appendix A

[62] The phase and amplitude information of complex EOF1 and EOF2 for SSTA and SSHA are shown in Figures A1 and A2, respectively. The time series of the variations of those complex EOF modes are also shown at the bottom of each figure. The phase diagram of the complex EOF1 demonstrates eastward phase propagation confirming the importance of oceanic Kelvin waves for El Niño.

Appendix B

[63] The partial correlation coefficient $r_{12.3}$ between two variables A_1, A_2, after removing the influence of the variable A_3, is given by

$$r_{12,3} = \frac{r_{12} - r_{13}\, r_{23}}{\sqrt{\left(1 - r_{13}^2\right)\left(1 - r_{23}^2\right)}} \tag{B1}$$

[64] In equation (B1) the term r_{ij} represents the linear correlation coefficient between A_i and A_j. The partial coefficient $r_{12.34}$ between two variables A_1, A_2, after removing the influence of the variables A_3 and A_4, is obtained by

$$r_{12,34} = \frac{r_{12,4} - r_{13,4}\, r_{23,4}}{\sqrt{\left(1 - r_{13,4}^2\right)\left(1 - r_{23,4}^2\right)}} = \frac{r_{12,3} - r_{14,3}\, r_{24,3}}{\sqrt{\left(1 - r_{14,3}^2\right)\left(1 - r_{24,3}^2\right)}} \tag{B2}$$

(equivalent to equation 7.2 of *Pedhazur* [1997]; also see *Ashok et al.* [2007]).

[65] The number of degrees of freedom for seasonal partial correlations was fixed at N-3 for the first order and N-4 for the second order, N being the number of values in the time series. Further details are available from, e.g., *Wilks* [1995], *Pedhazur* [1997], *Spiegel* [1997], and *Ashok et al.* [2007]. We also reconfirm the significance of the seasonal correlations over many regions of the globe by carrying out 1000 Monte Carlo simulations (broadly after *Saji and Yamagata* [2003]). To do this, we first generate 1000 sets of time series of random numbers which have the variance of the independent time series, such as EMI; the autocorrelation present in the original time series at Lag 1 is also preserved (for technical details, see *Broomhead and King* [1986], *Burg* [1978], *Marsaglia et al.* [1990], and *Vautard et al.* [1992]). These randomized time series are then used to compute the partial correlations with rainfall/temperature fields. After sorting the 1000 partial correlations, we designate the 900th highest value as the significant value at a 90% confidence level.

[66] We have also taken the autocorrelations of all the *monthly* time series into consideration when fixing the degrees of freedom for them [after *Davis*, 1976].

[67] **Acknowledgments.** The senior author (T.Y.) was encouraged by M. Yamamoto, a reporter of Kyodo News, to develop the present concept of ENSO Modoki in the early summer of 2004. The authors acknowledge Gary Meyers for the discussion on Australian droughts and J.-J. Luo for discussion on the decadal changes in the tropical Pacific. R. Lukas, J. McCreary, Z. Liu, H. Annamalai, and T. Tozuka are thanked for their helpful suggestions and comments on an earlier version. Constructive comments from three anonymous referees and James Richman helped to improve this manuscript. Useful comments from an anonymous reviewer of an earlier version are also acknowledged. The Pacific decadal oscillation index has been downloaded from http://www.atmos.washington.edu/~mantua/abst.PDO.html. Figures in this paper have been prepared using the GrADs (COLA), and FERRET software.

References

Aceituno, P. (1988), On the functioning of the Southern Oscillation in the South American sector, Part I: Surface climate, *Mon. Weather Rev.*, *116*, 505–525.

Adler, R. F., et al. (2003), The Version 2 Global Precipitation Climatology Project (GPCP) monthly precipitation analysis (1979–present), *J. Hydrometeorol.*, *4*, 1147–1167.

Allan, R. J., C. J. C. Reason, J. A. Lindesay, and T. J. Ansell (2003), 'Protracted' ENSO episodes and their impacts in the Indian Ocean region, *Deep Sea Res., Part II*, *50*, 2331–2347.

An, S.-I., and F.-F. Jin (2004), Non-linearity and asymmetry of ENSO, *J. Clim.*, *17*, 2399–2412.

Annamalai, H., J. Potemra, R. Murtugudde, and J. P. McCreary (2005), Effect of preconditioning on the extreme climate events in the tropical Indian Ocean, *J. Clim.*, *18*, 3450–3469.

Ashok, K., Z. Guan, and T. Yamagata (2001), Impact of the Indian Ocean dipole on the relationship between the Indian Monsoon rainfall and ENSO, *Geophys. Res. Lett.*, *28*, 4499–4502.

Ashok, K., Z. Guan, and T. Yamagata (2003), Influence of the Indian Ocean Dipole on the Australian winter rainfall, *Geophys. Res. Lett.*, *30*(15), 1821, doi:10.1029/2003GL017926.

Ashok, K., Z. Guan, N. H. Saji, and T. Yamagata (2004), Individual and combined influences of the ENSO and Indian Ocean Dipole on the Indian summer monsoon, *J. Clim.*, *17*, 3141–3155.

Ashok, K., H. Nakamura, and T. Yamagata (2007), Impacts of ENSO and IOD events on the Southern Hemisphere storm track activity during austral winter, *J. Clim.*, *20*, 3147–3163, doi:10.1175/JCLI4155.1.

Behera, S. K., and T. Yamagata (2001), Subtropical SST dipole events in the southern Indian Ocean, *Geophys. Res. Lett.*, *28*, 327–330.

Behera, S. K., J.-J. Luo, S. Masson, P. Delecluse, S. Gualdi, A. Navarra, and T. Yamagata (2005), Paramount impact of the Indian Ocean dipole on the East African short rains: A CGCM study, *J. Clim.*, *18*, 4514–4530.

Bjerknes, J. (1969), Atmospheric teleconnections from the equatorial Pacific, *Mon. Weather Rev.*, *97*, 163–172.

Broomhead, D. S., and G. King (1986), Extracting qualitative dynamics from experimental data, *Phys. D*, *20*, 217–236.

Burg, J. P. (1978), A new analysis technique for time series data, in *Modern Spectrum Analysis*, edited by D. G. Childers, pp. 42–48, IEEE Press, New York.

Carton, J. A., and B. S. Giese (2007), A reanalysis of ocean climate using SODA, *Mon. Weather Rev.*, in press.

Carton, J. A., B. S. Giese, and S. A. Grodsky (2005), Sea level rise and the warming of the oceans in the Simple Ocean Data Assimilation (SODA) ocean reanalysis, *J. Geophys. Res.*, *110*, C09006, doi:10.1029/2004JC002817.

Davis, R. E. (1976), Predictability of sea surface temperature and sea level pressure anomalies over the North Pacific Ocean, *J. Phys. Oceanogr.*, *6*, 249–266.

Deser, C., A. S. Phillips, and J. W. Hurrell (2004), Pacific interdecadal climate variability: Linkages between the tropics and the north Pacific during boreal winter since 1900, *J. Clim.*, *17*, 3109–3124.

Diaz, H. F., M. P. Hoerling, and J. K. Eischeid (2001), ENSO variability, teleconnections and climate change, *Int. J. Climatol.*, *21*, 1845–1862.

Donguy, J.-R., and A. Dessier (1983), El Niño-like events observed in the tropical Pacific, *Mon. Weather Rev.*, *111*, 2136–2139.

Enomoto, T., B. Hoskins, and Y. Masuda (2003), The formation of Bonin high in August, *Q. J. R. Meteorol. Soc.*, *587*, 157–178.

Fedorov, A. V., and S. G. Philander (2000), Is El Niño changing?, *Science*, *288*, 1997–2002.

Guan, Z., and T. Yamagata (2003), The unusual summer of 1994 in East Asia: IOD teleconnections, *Geophys. Res. Lett.*, *30*(10), 1544, doi:10.1029/2002GL016831.

Hartmann, B., and G. Wendler (2005), The significance of the 1976 Pacific climate shift in the climatology of Alaska, *J. Clim.*, *18*, 4824–4839.

Hoskins, B. J., and D. Karoly (1981), The steady liner response of a spherical atmosphere to thermal and orographic forcing, *J. Atmos. Sci.*, *38*, 1179–1196.

Inoue, M., and I. J. O'Brien (1987), Trends in sea level in the western and central equatorial Pacific during 1974–1975 to 1981, *J. Geophys. Res.*, *92*, 5045–5051.

Intergovernmental Panel on Climate Change (2001), *Climate Change 2001: Synthesis Report. A Contribution of Working Groups I, II, and III to the Third Assessment Report of the Intergovernmental Panel on Climate Change*, edited by R. T. Watson and the Core Writing Team, 398 pp., Cambridge Univ. Press, New York.

Jones, P. D., M. New, D. E. Parker, S. Martin, and I. G. Rigor (1999), Surface air temperature and its variations over the last 150 years, *Rev. Geophys.*, *37*, 173–199.

Kalnay, E., et al. (1996), The NCEP/NCAR 40-year reanalysis project, *Bull. Am. Meteorol. Soc.*, *77*, 437–471.

Kidson, J. W., M. J. Revell, B. Bhaskaran, A. B. Mullan, and J. A. Renwick (2002), Convection patterns in the tropical Pacific and their influence on the atmospheric circulation at high latitudes, *J. Clim.*, *15*, 137–159.

Kistler, R., et al. (2001), The NCEP-NCAR 50-year reanalysis: Monthly means CD-ROM and documentation, *Bull. Am. Meteorol. Soc.*, *82*, 247–268.

Kitamura, Y. (1990), Simulation of the annual and interannual variation of the tropical Pacific Ocean, *J. Mar. Syst.*, *1*, 169–181.

Larkin, N. K., and D. E. Harrison (2005a), On the definition of El Niño and associated seasonal average U.S. weather anomalies, *Geophys. Res. Lett.*, *32*, L13705, doi:10.1029/2005GL022738.

Larkin, N. K., and D. E. Harrison (2005b), Global seasonal temperature and precipitation anomalies during El Niño autumn and winter, *Geophys. Res. Lett.*, *32*, L16705, doi:10.1029/2005GL022860.

Levitus, S., J. Antonov, and T. Boyer (2005), Warming of the world ocean, 1955–2003, *Geophys. Res. Lett.*, *32*, L02604, doi:10.1029/2004GL021592.

Liu, Z., and B. Huang (2000), Cause of tropical Pacific warming trend, *Geophys. Res. Lett.*, *27*, 1935–1938.

Lohmann, K., and M. Latif (2005), Tropical Pacific decadal variability and the subtropical cells, *J. Clim.*, *18*, 5163–5178.

Luo, J., and T. Yamagata (2001), Long-term El Niño-Southern Oscillation (ENSO)-like variation with special emphasis on the South Pacific, *J. Geophys. Res.*, *106*, 22,211–22,228.

Mantua, N. J., S. R. Hare, Y. Zhang, J. M. Wallace, and R. C. Francis (1997), A Pacific interdecadal climate oscillation with impacts on salmon production, *Bull. Am. Meteorol. Soc.*, *78*, 1069–1079.

Marsaglia, G., A. Zaman, and W. W. Tsang (1990), Toward a universal random number generator, *Stat. Prob. Lett.*, *8*, 35–39.

McPhaden, M. J. (2004), lution of the 2002/03 El Niño, *Bull. Am. Meteorol. Soc.*, *85*, 677–695.

Meyers, S. D., J. J. O'Brien, and E. Thelin (1999), Reconstruction of monthly SST in the tropical Pacific Ocean during 1868–1993 using adaptive climate basis functions, *Mon. Weather Rev.*, *127*, 1599–1612.

Meyers, G., P. Mcintosh, L. Pigot, and M. Pook (2007), The years of El Niño, La Niña and interactions with the tropical Indian Ocean, *J. Clim.*, *20*, 2872–2880, doi:10.1175/JCLI4152.1.

Monahan, A. H., and A. Dai (2004), The spatial and temporal structure of ENSO non-linearity, *J. Clim.*, *17*, 3026–3036.

Nakamura, H., and A. Shimpo (2004), Seasonal variations in the Southern Hemisphere storm tracks and jet streams as revealed in a reanalysis dataset, *J. Clim.*, *17*, 1828–1844.

Namias, J., X. Yuan, and D. R. Cayan (1988), Persistence of North Pacific sea surface temperature and atmospheric flow patterns, *J. Clim.*, *1*, 682–703.

Navarra, A., M. N. Ward, and K. Miyakoda (1999), Tropical-wide teleconnections and oscillation. I: Teleconnection indices and type I/II states, *Q. J. R. Meteorol. Soc.*, *125*, 2909–2935.

Nitta, T. (1987), Convective activities in the tropical Pacific and their impacts on the Northern Hemisphere summer circulation, *J. Meteorol. Soc. Jpn.*, *65*, 373–390.

Nitta, T., and S. Yamada (1989), Recent warming of tropical sea surface temperature and its relationship to the Northern Hemisphere circulation, *J. Meteorol. Soc. Jpn.*, *67*, 375–383.

North, G. R., T. L. Bell, and R. F. Chalan (1982), Sampling errors in the estimation of empirical orthogonal functions, *Mon. Weather Rev.*, *110*, 699–706.

Pan, Y.-H., and A. H. Oort (1983), Global climate variations connected with sea surface temperature anomalies in the eastern equatorial Pacific Ocean for the 1958–73 period, *Mon. Weather Rev.*, *111*, 1244–1258.

Pedhazur, E. J. (1997), *Multiple Regression in Behavioural Research: Explanation and Prediction*, 3rd ed., Holt, Rinchart, and Winston, Austin, Tex.

Philander, S. G. H. (1990), *El Niño, La Niña and the Southern Oscillation,* 293 pp., Academic, San Diego, Calif.

Philander, S. G. H. (2004), *Our Affair With El Niño: How We Transformed an Enchanting Peruvian Current into a Global Climate Hazzard*, 296 pp., Princeton Univ. Press, Princeton, N. J.

Rao, S. A., and S. K. Behera (2005), Subsurface influence on SST in the tropical Indian Ocean: Structure and interannual variability, *Dyn. Atmos. Ocean*, *39*, 103–135.

Rao, S. A., and T. Yamagata (2004), Abrupt termination of Indian Ocean dipole events in response to intraseasonal disturbances, *Geophys. Res. Lett.*, *31*, L19306, doi:10.1029/2004GL020842.

Rao, S. A., S. Masson, J.-J. Luo, S. K. Behera, and T. Yamagata (2007), Termination of Indian Ocean dipole events in a general circulation model, *J. Clim.*, *20*, 3018–3035, doi:10.1175/JCLI4164.1.

Rasmusson, E. M., and T. H. Carpenter (1982), Variation in tropical sea surface temperature and surface wind fields associated with Southern Oscillation/El Niño, *Mon. Weather Rev.*, *110*, 354–384.

Rayner, N. A., D. E. Parker, E. B. Horton, C. K. Folland, L. V. Alexander, D. P. Rowell, E. C. Kent, and A. Kaplan (2003), Global analyses of sea surface temperature, sea ice, and night marine air temperature since the late nineteenth century, *J. Geophys. Res.*, *108*(D14), 4407, doi:10.1029/2002JD002670.

Reynolds, R. W., N. A. Rayner, T. M. Smith, D. C. Stokes, and W. Wang (2002), An improved in situ and satellite SST analysis for climate, *J. Clim.*, *15*, 1609–1625.

Richman, M. B. (1986), Rotation of principal components, *J. Climatol.*, *6*, 293–335.

Rodgers, K. B., P. Friederichs, and M. Latif (2004), Tropical Pacific decadal variability and its relationship to decadal modulations of ENSO, *J. Clim.*, *17*, 3761–3774.

Rodwell, M. J., and B. J. Hoskins (1996), Monsoons and the dynamics of deserts, *Q. J. R. Meteorol. Soc.*, *122*, 1385–1404.

Ropelewski, C. F., and M. S. Halpert (1987), North American precipitation and temperature patterns associated with the El Niño/Southern Oscillation (ENSO), *Mon. Weather Rev.*, *114*, 2352–2362.

Saji, N. H., and T. Yamagata (2003), Possible impacts of Indian Ocean dipole events on global climate, *Clim. Res.*, *25*, 151–169.

Saji, N. H., B. N. Goswami, P. N. Vinayachandran, and T. Yamagata (1999), A dipole mode in the tropical Indian Ocean, *Nature*, *401*, 360–363.

Saji, N. H., T. Ambrizzi, and S. E. T. Ferraz (2005), Indian Ocean dipole mode events and austral surface air temperatures, *Dyn. Atmos. Ocean*, *39*, 87–102.

Simmons, A. J., and J. K. Gibson (2000), The ERA-40 project plan, *ERA-40 Proj. Rep. Ser. 1*, 63 pp., Eur. Cent. for Medium-Range Weather Forecast., Reading, U. K.

Spiegel, M. R. (1997), *Schaum's Outline of Theory and Problems of Statistics*, McGraw-Hill, New York.

Stephens, C., S. Levitus, J. Antonov, and T. Boyer (2001), The Pacific regime shift, *Geophys. Res. Lett.*, *28*, 3721–3724.

Tozuka, T., and T. Yamagata (2003), Annual ENSO, *J. Phys. Oceanogr.*, *33*, 1564–1578.

Trenberth, K. E., and D. P. Stepaniak (2001), Indices of El Niño evolution, *J. Clim.*, *14*, 1697–1701.

Trenberth, K. E., G. W. Branstator, D. Karoly, A. Kumar, N.-C. Lau, and C. Ropelewski (1998), Progress during TOGA in understanding and modeling global teleconnections associated with tropical sea surface temperatures, *J. Geophys. Res.*, *103*, 14,291–14,324.

Trenberth, K. E., D. P. Stepaniak, J. W. Hurrell, and M. Fiorino (2001), Quality of reanalyses in the tropics, *J. Clim.*, *14*, 1499–1510.

Trenberth, K. E., D. P. Stepaniak, and J. M. Caron (2002a), Interannual variations in the atmospheric heat budget, *J. Geophys. Res.*, *107*(D8), 4066, doi:10.1029/2000JD000297.

Trenberth, K. E., J. M. Caron, D. P. Stepaniak, and S. Worley (2002b), The evolution of El Niño-Southern Oscillation and global atmospheric

temperatures, *J. Geophys. Res.*, *107*(D8), 4065, doi:10.1029/2000JD000298.
Vautard, R., P. Yiou, and M. Ghil (1992), Singular spectrum analysis: A toolkit for short, noisy, chaotic time series, *Physics D*, *58*, 95–126.
Walker, G. T. (1923), Correlations in seasonal variations of weather, VIII. A preliminary study of world weather I, *Mem. India Meteorol. Dep.*, *23*, 75–131.
Walker, G. T. (1924), Correlations in seasonal variations of weather, IX, *Mem. India Meteorol. Dep.*, *24*, 275–332.
Wang, B., R. Wu, and T. Li (2003), Atmosphere-warm ocean interaction and its impact on Asian-Australian monsoon variability, *J. Clim.*, *16*, 1195–1211.
Weare, B. C., A. R. Navato, and R. E. Newell (1976), Empirical orthogonal analysis of Pacific sea surface temperatures, *J. Phys. Oceanogr.*, *6*, 671–678.
Webster, P. J. (1982), Seasonality in the local and remote atmospheric response to sea surface temperatures, *J. Atmos. Sci.*, *39*, 41–52.
Weng, H., K. Ashok, S. K. Behera, S. A. Rao, and T. Yamagata (2007), Impacts of recent El Niño on Modoki dry/wet conditions in the Pacific rim during boreal summer, *Clim. Dyn.*, *29*, 113–129, doi:10.1007/s00382-007-0234-0.
Wilks, D. S. (1995), *Statistical Methods in the Atmospheric Sciences: An Introduction*, 467 pp., Academic, San Diego, Calif.
Xie, P., and P. A. Arkin (1996), Analyses of global monthly precipitation using rain gauge observations, satellite estimates and numerical model predictions, *J. Clim.*, *9*, 840–858.
Yamagata, T., and Y. Masumoto (1992), Interdecadal natural climate variability in the western Pacific and its implication in global warming, *J. Meteorol. Soc. Jpn.*, *70*, 167–175.
Yamagata, T., S. K. Behera, J.-J. Luo, S. Masson, M. R. Jury, and S. A. Rao (2004), The coupled ocean-atmosphere variability in the tropical Indian Ocean, in *Earth's Climate: The Ocean-Atmosphere Interaction*, *Geophys. Monogr. Ser.*, vol. 147, edited by C. Wang et al., pp. 189–211, AGU, Washington, D. C.
Yin, X., A. Gruber, and P. Arkin (2004), Comparison of the GPCP and CMAP Merged Gauge-Satellite monthly precipitation products for the period 1979–2001, *J. Hydrometeorol.*, *5*, 1207–1222.
Zhang, Y., J. M. Wallace, and D. S. Battisti (1997), ENSO-like interdecadal variability: 1900–93, *J. Clim.*, *10*, 1004–1020.

K. Ashok, APEC Climate Center, National Pension Corporation Busan Building 12F, Yeonsan 2-dong, Yeonje-gu, Busan 611705, South Korea. (ashok@apcc21.net)

S. K. Behera, S. A. Rao, and H. Weng, Frontier Research Center for Global Change/JAMSTEC, 3173-25, Showamachi, Kanazawa-Ku, Yokohama, Kanagawa 236-0001, Japan. (behera@jamstec.go.jp; scrao@jamstec.go.jp; weng@jamstec.go.jp)

T. Yamagata, Department of Earth and Planetary Science, Graduate School of Science, University of Tokyo, Hongo 7-3-1, Bunkyo-ku, Tokyo 113-0033, Japan. (yamagata@eps.s.u-tokyo.ac.jp)